Model-Based Dynamic Positioning of Underwater Robotic Vehicles: Theory and Experiment

David A. Smallwood, *Member, IEEE,* and Louis L. Whitcomb, *Senior Member, IEEE*

***Abstract*—This paper addresses the trajectory tracking problem for the low-speed maneuvering of fully actuated underwater vehicles. It is organized as follows. First, a brief review of previously reported control studies and plant models is presented. Second, an experimentally validated plant model for The Johns Hopkins University Remotely Operated Underwater Vehicle (JHUROV) is reviewed. Third, the stability of linear proportional-derivative (PD) control and a family of fixed and adaptive model-based controllers is examined analytically and demonstrated with numerical simulations. Finally, we report results from experimental trials comparing the performance of these controllers over a wide range of operating conditions. The experimental results corroborate the analytical predictions that the model-based controllers outperform PD control over a wide range of operating conditions. The exactly linearizing model-based controller is outperformed by its nonexactly linearizing counterpart. The adaptive controllers are shown to provide reasonable online plant parameter estimates, as well as velocity and position tracking consistent with theoretical predictions—providing good velocity tracking and, with the appropriate parameter update law, position tracking. The effects of reference trajectory, "bad" model parameters, feedback gains, adaptation gains, and thruster saturation are experimentally evaluated. To the best of our knowledge, this is the first reported comparative experimental study of this class of model-based controllers for underwater vehicles.**

***Index Terms*—Adaptive control, asymptotic stability, control systems, proportional control, nonlinear control, underwater vehicles, underwater vehicle control, underwater vehicle propulsion, underwater vehicle testing.**

I. Introduction

THE problem addressed in this paper, the *trajectory tracking problem* for the low-speed maneuvering of fully actuated underwater vehicles, is defined as follows. Given an underwater vehicle plant and a continuous bounded time-varying reference trajectory whose derivatives are continuous and bounded, design a controller that ensures that the plant state converges asymptotically to the reference trajectory.

Finite-dimensional approximate plant models for the dynamics of underwater vehicles are structurally similar to the equations of motion for fully actuated holonomic rigid-body mechanical system—both classes of plants posses nonlinear (NL) dynamics—yet their plant parameters (e.g., mass, inertia, drag, friction) enter linearly into the overall NL differential equation of motion. For the special case of second-order mechanical systems with *linear* dynamics, classical linear controller design techniques apply directly. Early studies of trajectory tracking for NL plant dynamics arising in rigid-body holonomic mechanical systems employed linearized plant approximations in order to apply linear control techniques [18], [35], [58].

The controllers reported herein are motivated by the structure of previously reported model-based approaches to the problem of exactly controlling fully NL holonomic mechanical systems. These tracking controllers have generally employed one of the three following general approaches.

1) **Linear Control—Proportional Derivative (PD) and Proportional Integral Derivative (PID):** The globally asymptotic regulation of a fully NL mechanical system was first addressed for PD control of robot arms in [6], in which Lasalle's Invariance Theorem [42] is employed to show that PD control provides globally asymptotic setpoint regulation. The application of this approach to the control of underwater vehicles is the PD controller outlined in Section III-A.
2) **NL Model-Based Exact Linearization:** The case of exact model-based trajectory tracking control of robot arms was first reported independently in [25], [45], and [46], which report controllers with model-based feedforward terms that employ feedback linearization to exactly linearize the plant (without any approximation) and result in globally asymptotically stable linear error dynamics. Working implementations of this approach were first reported in [2]. An adaptive version of this exact linearization approach was reported in [12] and [13] and have been shown to be globally asymptotically stable in tracking error and locally stable in plant parameter error.

   The application of this approach to the control of underwater vehicles is the *exact linearizing* (EL) controller outlined in Section III-B and the *adaptive exact linearizing* (AEL) controller outlined in Section III-D.
3) **NL Model-Based Without Linearization:** The case of exact model-based tracking of robot arms *without exact linearization* is reported in [51]–[53] and [62], along with adaptive extensions that are globally asymptotically stable in tracking error and globally stable in plant parameter error.

   The application of this approach to the control of underwater vehicles is the NL controller outlined in Section III-C, the *adaptive NL* (ANL) controller outlined in Section III-E, and the *epsilon adaptive NL* (ϵANL) controller of Section III-F.

Manuscript received October 9, 2001; revised August 19, 2003. This work was supported by the Office of Naval Research and by the National Science Foundation under Grant CMS-0100783.

The authors are with the Department of Mechanical Engineering, The Johns Hopkins University, Baltimore, MD 21218 USA (e-mail: smallwood@jhu.edu; llw@jhu.edu).

Digital Object Identifier 10.1109/JOE.2003.823312

For the special problem of trajectory tracking of underwater vehicles, a significant number of previously reported studies have employed linearized plant approximations both for the theoretically justified case of setpoint regulation and the theoretically unjustified case of trajectory tracking. In [28], the authors report a linear discrete-time approximation for vehicle dynamics and report numerical simulation of linear quadratic and robust control methods for this class of discrete time linear plants. In [29] and [40], the authors report linear quadratic control and self-tuning control of linearized plant models and numerical simulations. In [15] and [36], the authors report PI and linear model-reference adaptive control of a linearized plant model and experimental demonstrations. In [31] and [33], the authors report the model-reference adaptive control of a linearized plant models and numerical simulations. In [14], the authors report the sliding-mode control of a linearized plant models and numerical simulations.

Several studies, e.g., [38], have reported neural network and/or fuzzy logic control technique and numerical simulations. Numerous reported control studies demonstrate the performance of proposed closed-loop systems in computer simulations alone, e.g., [3], [14], [29] and [60], or employ nonparametric control methodologies that do not require knowledge of the plant dynamics [10].

Relatively few control studies directly address decoupled NL plant models for underwater vehicles. In [64], the authors report NL sliding mode control and numerical simulations for X, Y, and heading. The first experimental evaluation of NL adaptive sliding-mode model-based control on underwater vehicles was reported in [63]. In [5], [10], and [65], the authors report on the experimental performance of model-based adaptive controllers for underwater vehicles.

In [8], the authors address the problem of model-based vehicle state estimation. Several reported studies address the highly idealized special case of propulsionless, appendageless, and symmetric vehicles in inviscid fluid for which the partial differential equations governing the motion of the surrounding fluid have a closed-form solution, e.g., [44].

Several studies address fully coupled NL plant models and controllers and report simulation studies, e.g., [4], [5], [23], and [24]. These approaches typically make explicit assumptions on the structure of the approximate finite-dimensional vehicle plant dynamics to ensure that the vehicle plant model possesses passivity properties identical to those possessed by rigid-body holonomic mechanical systems—an assumption that has not been widely empirically validated for the class of underwater robotic vehicles described herein.

A. Review of Dynamical Modeling of Underwater Vehicles

Exact analysis of a rigid-body underwater vehicle's dynamics includes both the finite-dimensional dynamic of the vehicle body itself and the infinite-dimensional dynamics of the fluid surrounding the vehicle. The former is a finite-dimensional dynamical system represented by an ordinary differential equation (ODE), but the latter is a continuous (infinite-dimensional) dynamical system represented by the incompressible Navier–Stokes equations, a partial differential equation (PDE). Except for a few idealized cases of little practical utility (e.g., symmetric bodies in inviscid fluid) for which the PDE fluid component has a closed-form solution, the numerical solution of the full vehicle (ODE) and fluid (PDE) dynamical system remains a formidable computational obstacle and an area of active research [41].

The overwhelming computational complexity of PDE dynamical models has motivated the widespread use (by naval architects and others) of finite-dimensional *approximate* models for marine vehicles, sometimes termed "lumped parameter models." The expedient of experimentally determining approximate finite-dimensional models for complex fluid phenomenon is widely employed in naval architecture. The most commonly accepted finite-dimensional dynamics models for *submarine vehicles* trace their lineage to studies performed at the U.S. Navy's David Taylor Model Basin, beginning in the 1950s [26], [30], with subsequent revisions reported in [21] and [22]. These second-order NL ODE dynamical models are known as the DTMB standard submarine equations of motion and subsequent enhancements have been adopted for use in the design of control systems for underwater robotic vehicles, in either linearized form, e.g., [31] or full NL form, e.g., [33].

Most reported finite-dimensional plant models for underwater vehicles take the general form

$$\tau_p(t) = M(x_w(t), v_p(t))\dot{v}_p(t) + d(x_w(t), v_p(t)) + b(x_w(t)) \tag{1}$$

where $x_w(t) \in \mathbb{R}^{6x1}$ is a vector of the vehicle position and orientation in world inertial coordinates; $v_p(t) \in \mathbb{R}^{6x1}$ and $\dot{v}_p(t) \in \mathbb{R}^{6x1}$ are, respectively, vectors of the vehicle velocity and acceleration in vehicle body coordinates; $\tau_p(t) \in \mathbb{R}^{6x1}$ is a vector of control forces and moments generated by thrusters and control surfaces in body coordinates; $M(x_w(t), v_p(t))$ is a mass matrix representing both rigid-body mass and velocity-dependent "added mass"; $d(x_w(t), v_p(t))$ is a vector of vehicle drag and coriolis forces; and $b(x_w(t))$ is a vector of vehicle buoyancy forces. Note that the velocity in inertial (world) coordinates $v_w(t)$ is related to the velocity in body coordinates by a linear transformation of the form $v_w(t) = T(x_w(t))\ v_p(t)$ [26]. The plant (1) can also be rewritten as

$$\begin{aligned}\dot{v}_p(t) = {} & M(x_w(t), v_p(t))^{-1}\tau_p(t) \\ & - M(x_w(t), v_p(t))^{-1}d(x_w(t), v_p(t)) \\ & - M(x_w(t), v_p(t))^{-1}b(x_w(t)).\end{aligned} \tag{2}$$

At present, there is no uniform consensus within the research community on the exact analytical form of the terms comprising $M(x_w(t), v_p(t))$, $d(x_w(t), v_p(t))$, and $b(x_w(t))$, nor for the force vector $\tau_p(t)$. The few studies that have reported specific instances of (1), e.g., [33], have based their component terms on the DTMB standard submarine equations of motion [22], [26].

Although not theoretically justified, in this report we adopt the common practice of further approximating the six degree-of-freedom (DOF) equations by neglecting off diagonal entries and coupling terms, tether dynamics, as well as assuming a constant added mass [9], [49]. The resulting decoupled single-DOF dynamical equations take the form

$$\tau_i(t) = m_i\dot{v}_i(t) + d_{Q_i}v_i(t)|v_i(t)| + d_{L_i}v_i(t) + b_i, \quad m_i > 0; d_{L_i}, d_{Q_i} > 0 \tag{3}$$

TABLE I
NOMENCLATURE

Degree of Freedom	Force Moment (Body Coord.)	Linear Velocity Angular Velocity (Body Coord.)	Linear Position Angular Position (World/Inertial Coord.)
1: X Translation (Surge)	$\tau_1(t)[N]$	$v_1(t)[m/s]$	$x_1(t)[m]$
2: Y Translation (Sway)	$\tau_2(t)[N]$	$v_2(t)[m/s]$	$x_2(t)[m]$
3: Z Translation (Heave)	$\tau_3(t)[N]$	$v_3(t)[m/s]$	$x_3(t)[m]$
4: Rotation About Z(Yaw/HDG)	$\tau_4(t)[N-m]$	$v_4(t)[rad/s]$	$x_4(t)[rad]$
5: Rotation About Y(Pitch)	$\tau_5(t)[N-m]$	$v_5(t)[rad/s]$	$x_5(t)[rad]$
6: Rotation About X(Roll)	$\tau_6(t)[N-m]$	$v_6(t)[rad/s]$	$x_6(t)[rad]$

TABLE II
LUMPED PARAMETERS

Lumped Parameters	Physical Definition	Units DOF 1,2, and 3	DOF 4
α_i	m_i^{-1}	[1/kg]	[rad/(kg m^2)]
β_i	$-m_i^{-1}d_{Q_i}$	[1/m]	[rad]
μ_i	$-m_i^{-1}d_{L_i}$	[1/s]	[1/s]
ν_i	$-m_i^{-1}b_i$	[m/s^2]	[rad/s^2]

or rewritten as

$$\dot{v}_i(t) = m_i^{-1}\tau_i(t) - m_i^{-1}d_{Q_i}v_i(t)|v_i(t)| - m_i^{-1}d_{L_i}v_i(t) - m_i^{-1}b_i \quad (4)$$

where, for each DOF i, $\tau_i(t)$ is the net control force, m_i is the effective mass, $d_{Q_i}v_i(t)|v_i(t)|$ and $d_{L_i}v_i(t)$ represent the hydrodynamic drag, and b_i is the buoyancy. Note that these equations are written in the body-fixed coordinates and that we have dropped the subscript indicating so for the remainder of this paper. Using lumped parameters, (4) can be written as

$$\dot{v}_i(t) = \alpha_i\tau_i + \beta_i v_i(t)|v_i(t)| + \mu_i v_i(t) + \nu_i. \quad (5)$$

The decoupled single DOF, lumped parameter, dynamical plant model can be written in vector form as

$$\dot{v}(t)_i = \Phi_i^T f(t)_i \quad (6)$$

where $\Phi_i = [\alpha_i; \beta_i; \mu_i; \nu_i]_{4\times 1}$ is the vector of lumped plant parameters and $f(t)_i = [\tau(t)_i; v_i(t)|v_i(t)|; v_i(t); 1]_{4\times 1}$ is a NL vector of state and the control input $\tau(t)_i$. The lumped parameters are defined in Table II. A complete detailed derivation of the equations of motion can be found in [55].

We adapt the Naval Architecture convention in Table I. Linear position in the x_1, x_2, and x_3 DOFs is given with respect to a fixed inertial coordinate frame. Vehicle velocity and acceleration in the x_1, x_2, and x_3 DOFs are with respect to a body-coordinate frame. Again, note that the velocity in inertial (world) coordinates $v_w(t)$ is related to the velocity in body coordinates by a linear transformation of the form $v_w(t) = T(x_w(t))v(t)$ [26]. Euler angles are used to represent the angular position in the x_4, x_5, and x_6 DOFs. The authors recognize that the Euler angle representation possesses singularities. In general, however, underwater robotic vehicles such as The Johns Hopkins University Remotely Operated Vehicle (JHUROV) experience small to moderate pitch and roll motion; thus, they are not physically attaining values to cause singularities in the representation of the vehicles orientation.

B. Review of Plant Model Parameter Identification Methods for Underwater Vehicles

Several methods of determining the parameters of dynamical equations of motion for underwater vehicles have been presented in the literature. These include the method of least-squares [9], [19], [27] and the use of extended Kalman filters (EKF) [1], [19]. A method based on numerical minimization of the error between the trajectories of the vehicle and several models during free decay, in 1-DOF, was presented in [49].

Relatively few studies, e.g., [32] and [63], have reported experiments that experimentally identify the plant parameters for dynamical plant models in multiple DOFs; even fewer studies, such as [9], [49], [56], and [57], report both experimentally determined model parameters *and* compare experimentally observed vehicle dynamical response with that predicted by the proposed analytical models.

This paper reports a direct comparison of the performance of model-based controllers employing (1) plant parameters obtained offline, as noted above, and (2) plant parameters obtained online with the adaptive controllers reported herein and also investigates the effect of "bad" model parameters on system tracking performance.

C. Review of Dynamic Positioning of Marine Vehicles

The first automatic control system for marine vehicles was the "Sperry Gyropilot for Ships" heading autopilot developed by Sperry Corporation in 1922 [48]. These empirically tuned systems employed PD and, subsequently, PID controllers to automatically steer a vessel on a constant heading. With the advent of reliable marine inertial navigation systems in the 1950s [43], satellite radio navigation methods (LORAN-C in the 1960s [17] and the Navstar global positioning system (GPS) in the 1980s [20]), the role of marine autopilots expanded to provide track-line following, way-point navigation, and great-circle routing [48].

Before the 1970s, control systems for marine vehicles were exclusively designed for heading, speed, and track-line control for surface vessels. The design of these control systems has been almost exclusively based on linear control theory and linearized plant models of vehicle dynamics operating at a nominal advance velocity (speed). This approach of employing linearized plant models is exemplified both in early studies of heading control, e.g., [16], and recent reports employing adaptive techniques for automatic heading and roll control [59].

TABLE III
ADAPTIVE ID LUMPED PARAMETERS

degree-of-freedom	α_i	β_i	μ_i	ν_i	Error e_i
1 (x_1)	0.003755 [1/kg]	-4.406 [1/m]	0 [1/s]	0.007358 [m/s^2]	0.01664 m/s
2 (x_2)	0.002355 [1/kg]	-4.9952[1/m]	0 [1/s]	-0.004066 [m/s^2]	0.01607 m/s
3 (x_3)	6.237e-4 [1/kg]	-1.102 [1/m]	0 [1/s]	0.01934 [m/s^2]	0.01652 m/s
4 (x_4)	0.0102 [rad/(kg m^2)]	-1.9086[rad]	0 [1/s]	-0.001221[rad/s^2]	.0288 rad/s
degree-of-freedom	Inertia	D_Q	D_L	Buoyancy	
1 (x_1)	266.3 [kg]	1173.4 [kg/m]	0 [kg/s]	-1.96 [N]	
2 (x_2)	424.6 [kg]	2120.9 [kg/m]	0 [kg/s]	1.73 [N]	
3 (x_3)	1603.3[kg]	1766.84[kg/m]	0 [kg/s]	-31.01 [N]	
4 (x_4)	98.04 [(kg m^2)/rad]	187.1 [kg m^2]	0 [(kg m^2)/(rad s)]	0.1197 [N-m]	

The development [37] and commercialization of long-baseline (LBL) acoustic navigation in the 1970s provided the ability to measure the position of a marine vehicle with unprecedented precision (1–10 m) and update rate (0.1–1.0 Hz) [11], [47]. This enabled, for the first time, closed-loop automatic control of marine vehicles for low-speed maneuvering and stationkeeping. The industry has adopted the term *dynamic positioning* (DP) for fully actuated automatic control of low-speed maneuvering and stationkeeping, as distinguished from automatic heading and speed control.

Most dynamically positioned marine vehicles in use today employ PD or PID controllers for each controlled DOF of the form

$$\vec{\tau}_d = K_p \Delta\vec{x}_p + K_d \Delta\vec{v}_p + K_i \int_0^t \Delta\vec{x}_p(\sigma)d\sigma \qquad (7)$$

where $\Delta\vec{x}_p$ and $\Delta\vec{v}_p$ are the position and velocity tracking error vectors, respectively, in body coordinates; K_p, K_i, and K_d are empirically tuned feedback gain matrices; and $\vec{\tau}_d$ is the vector of net forces and moments commanded to the vehicle thruster system.

These PID control algorithms are designed with the simplifying assumption that the "plant" is a second-order linear time-invariant dynamical system and that the "disturbance terms" of hydrodynamic forces, wind, and sea state are constant. It is easy to show theoretically that the PID controllers will provide set-point regulation (stationkeeping) if the plant is linear and the disturbances are constant. For the case of trajectory tracking, however, the PID controller cannot provide exact tracking (either in theory or practice) even for a linear second-order plant. Moreover, PID control cannot dynamically compensate for unmodeled vehicle hydrodynamic forces and "unknown" variations in disturbances of current, wind, and sea state as the vessel tracks a trajectory. Although some commercially available dynamic-positioning ship controllers employ "model-based" compensation for wind force and desired acceleration, most do not. The principal reason that model-based compensation is *not* widely used is that the required plant models are unavailable and the associated plant parameters are difficult to estimate with any accuracy and, consequencely, in practice they are empirically tuned by trial and error.

II. DECOUPLED DYNAMICAL PLANT MODEL FOR THE JHUROV

This section reviews an experimentally identified, decoupled, single-DOF dynamical plant models of the form (4) for the JHUROV. A set of plant model parameters was identified for the x_1, x_2, x_3, and x_4 DOFs using a stable adaptive identifier, originally reported in [57]. The scalar adaptive identifier was run on the experimental data, collected by conducting dynamic vehicle trials in which the JHUROV was commanded to follow an open-loop sinusoidal thrust profile. The output of this process is an estimated plant velocity, $\hat{v}(t)_i$, as well as estimates for the unknown plant parameters. The adaptively identified plant parameter values agree closely with those obtained from the experimental data using a least-square parameter identification method.

How well does the identified plant model performance agree with experimentally observed actual vehicle motion? To answer this question, we ran simulations on the adaptively identified plant parameters, in each DOF i. The simulation used the logged commanded force profile that the JHUROV experienced during the experimental trials and the identified plant parameters to predict the dynamical motion of the JHUROV. The output of the simulations was a velocity v_{model_i}. The logged experimental plant velocity v_{p_i} was then compared to the velocity predicted by the dynamical plant model v_{model_i}. The error for each DOF i is calculated as $e_i = \mathrm{mean}(|v_{\mathrm{model}_i} - v_{p_i}|)$. The best identified parameters were those with the lowest "error" and are listed in Table III.

As seen by the error listed in Table III, the identified dynamical plant models were able to predict the dynamical behavior of the JHUROV down to 1.6 cm/s in the x_1, x_2, and x_3 DOF and 0.0288 rad/s in the x_4 DOF. A detailed evaluation of this plant model is reported in [57].

The buoyant force term represents a combination of the actual buoyancy force and unmodeled dynamics. One note is that the only significant nonzero buoyancy term is found in the x_3 DOF. The nonzero values in the other DOF are most likely attributed to nonzero thruster command offset in the thruster control subsystem.

III. MODEL-BASED TRACKING CONTROL ALGORITHMS: THEORY AND SIMULATION

In this section we present five different model-based controllers and a basic PD controller. The form of each controller is presented followed by a stability analysis of the resulting closed-loop dynamical system. The model-based controllers were designed to track both position and velocity trajectories. The remainder of this section reports these control algorithms and examines their stability when in closed-loop control of plants of the general form (4).

A. PD Controller

The basic PD controller for a single-DOF plant takes the form

$$\tau(t) = k_p \Delta x(t) + k_d \Delta v(t), \quad k_p, k_d > 0 \tag{8}$$

where k_p and k_d are scalar error feedback gains. The state error coordinates are defined as

$$\begin{aligned} \Delta x(t) &= x_d(t) - x_p(t), \\ \Delta v(t) &= v_d(t) - v_p(t), \\ \Delta \dot{v}(t) &= \dot{v}_d(t) - \dot{v}(t) \end{aligned} \tag{9}$$

where $\dot{v}_d(t)$, $v_d(t)$, and $x_d(t)$ are the desired acceleration, velocity, and position. $x_p(t)$ and $v_p(t)$ are the actual plant position and velocity. Substituting (8) into (3), the resulting closed-loop dynamical system is

$$0 = m\dot{v}_p(t) + d_Q v_p(t)|v_p(t)| + d_L v_p(t) + b - k_p \Delta x(t) - k_d \Delta v(t). \tag{10}$$

In the case where the buoyancy term b is zero, an application of Lasalle's Invariance Theorem [42] shows that the PD controller will perform setpoint regulation, but not trajectory tracking [6].

While the PD controller does not perform trajectory tracking, it was included because it represents the most widely used controller in use in the world and, as such, represents a baseline to compare the performances of the model-based controllers.

B. EL Model-Based Controller

The EL model-based controller for a single-DOF system takes the form

$$\begin{aligned} \tau(t) &= m\dot{v}_d(t) + d_Q v_p(t)|v_p(t)| \\ &\quad + d_L v_d(t) + b + k_p \Delta x(t) + k_d \Delta v(t), \\ m, k_p, k_d &> 0, \quad d_Q, d_L \geq 0 \end{aligned} \tag{11}$$

where m, d_Q, d_L, and b are known scalar quantities; $\tau(t)$ is the controller output; and k_p and k_d are PD scalar error feedback gains. The state error coordinates are defined in (9). Substituting (11) into (3), the resulting closed-loop dynamical system is

$$m\Delta\dot{v}(t) + (d_L + k_d)\Delta v(t) + k_p \Delta x(t) = 0 \tag{12}$$

a linear system that is time invariant in the error coordinates.

As defined, d_L, k_p, and k_d are positive constants; therefore, the closed-loop dynamical system (12) has a globally asymptotically stable equilibrium point at the origin $(\Delta x(t), \Delta v(t) = 0)$. We conclude that $\lim_{t\to\infty} \Delta x(t) = 0$ and $\lim_{t\to\infty} \Delta v(t) = 0$. This controller is an application to underwater vehicles of the general methodology originally reported in [25], [45], and [46].

C. NL Model-Based Controller

The NL model-based controller for a single DOF takes the form

$$\begin{aligned} \tau(t) &= m\dot{v}_d(t) + d_Q v_d(t)|v_d(t)| \\ &\quad + d_L v_d(t) + b + k_p \Delta x(t) + k_d \Delta v(t), \\ m, k_p, k_d &> 0, \quad d_Q, d_L \geq 0 \end{aligned} \tag{13}$$

where m, d_Q, d_L, and b are known scalar quantities; $\tau(t)$ is the controller output; and k_p and k_d are PD scalar error feedback gains. The state error coordinates are defined in (9). Substituting (13) into (3), the resulting closed-loop dynamical system is

$$0 = m\Delta\dot{v}(t) + d_Q(v_d(t)|v_d(t)| - v_p(t)|v_p(t)|) + (d_L + k_d)\Delta v(t) + k_p \Delta x(t) \tag{14}$$

or rewritten as

$$\Delta\dot{v}(t) = -m^{-1}(d_Q(v_d(t)|v_d(t)| - v_p(t)|v_p(t)|) + (d_L + k_d)\Delta v(t) + k_p \Delta x(t)). \tag{15}$$

Consider the Lyapunov function candidate

$$W(\Delta v(t), \Delta x(t)) = \frac{1}{2} k_p \Delta x(t)^2 + \frac{1}{2} m \Delta v(t)^2. \tag{16}$$

The time derivative of (16) is

$$\dot{W}(\Delta v(t), \Delta x(t)) = -(d_L + k_d)\Delta v(t)^2 - d_Q(v_d(t)|v_d(t)| - v_p(t)|v_p(t)|)\Delta v(t). \tag{17}$$

Examining the term $(v_d(t)|v_d(t)| - v_p(t)|v_p(t)|)\Delta v(t)$, we see that when $\Delta v(t) > 0$ we have $v_p(t) < v_d(t)$, which results in $(v_d(t)|v_d(t)| - v_p(t)|v_p(t)|) > 0$ and $(v_d(t)|v_d(t)| - v_p(t)|v_p(t)|)\Delta v(t) > 0$. Likewise, if $\Delta v(t) < 0$, then we have $v_p(t) > v_d(t)$, resulting in $(v_d(t)|v_d(t)| - v_p(t)|v_p(t)|) < 0$ and $(v_d(t)|v_d(t)| - v_p(t)|v_p(t)|)\Delta v(t) > 0$. Thus, (17) is negative semidefinite. The resulting closed-loop system, shown in (14), has an equilibrium point at the origin $(\Delta x(t), \Delta v(t) = 0)$ that is globally stable. Therefore, both $\Delta x(t)$ and $\Delta v(t)$ are bounded. We conclude with the following points.

1) $\Delta x(t)$ and $\Delta v(t)$ are bounded.
2) Since we define $v_d(t)$ and $x_d(t)$ to be bounded signals, as a result of point 1 both $v_p(t)$ and $x_p(t)$ are bounded.
3) As a consequence of point 2) and $m \neq 0$, we get from (15) that $\Delta\dot{v}(t)$ is bounded.
4) Given (17) and that $d_Q(v_d(t)|v_d(t)| - v_p(t)|v_p(t)|)\Delta v(t) \geq 0$ as argued earlier, we get $\Delta v(t)^2 \leq -W(\Delta v(t), \Delta x(t))/(d_L + k_d)$.
5) Given that $\Delta v(t)$ is bounded from point 1), then $||\Delta v(t)|| = (\int_0^\infty |\Delta v(t)|^2\, dt)^{1/2}$ exists and is finite. Thus, $\Delta v(t) \in L^2$.
6) Using [50, Corollary 2.9] with points 3) and 5), $\lim_{t\to\infty} \Delta v(t) = 0$.

In summary, we conclude that all signals remain bounded and that the velocity error asymptotically tracks to zero. This approach is an application to underwater vehicles of the general methodology originally reported in [52], [53], and [62].

D. AEL Model-Based Controller

The AEL for a single DOF takes the form

$$\begin{aligned} \tau(t) &= \hat{m}(t)\dot{v}_d(t) + \hat{d}_Q(t) v_p(t)|v_p(t)| + \hat{d}_L(t) v_d(t) \\ &\quad + \hat{b}(t) + k_p \Delta x(t) + k_d \Delta v(t), \\ k_p, k_d &> 0 \end{aligned} \tag{18}$$

where $\hat{m}(t)$, $\hat{d}_Q(t)$, $\hat{d}_L(t)$, and $\hat{b}(t)$ are adaptive estimates of the scalar plant parameter values; $\tau(t)$ is the controller output;

and k_p and k_d are PD scalar error feedback gains. The plant parameter error coordinates are defined as

$$\begin{aligned}\Delta m(t) &= \hat{m}(t) - m \\ \Delta d_Q(t) &= \hat{d}_Q(t) - d_Q \\ \Delta d_L(t) &= \hat{d}_L(t) - d_L \\ \Delta b(t) &= \hat{b}(t) - b, \\ \Delta\Psi(t) &= \hat{\Psi}(t) - \Psi \\ \Delta\dot{\Psi}(t) &= \dot{\hat{\Psi}}(t); \quad \dot{\Psi} = 0 \end{aligned} \tag{19}$$

where $\hat{\Psi}(t) = [\hat{m}(t); \hat{d}_Q(t); \hat{d}_L(t); \hat{b}(t)]_{4\times 1}$ is an estimate of the unknown plant parameter vector $\Psi = [m; d_Q; d_L; b]_{4\times 1}$. Substituting (18) into (3), the resulting closed-loop dynamical system is

$$\begin{aligned}0 = {} & \Delta m(t)\dot{v}_d(t) + \Delta d_Q(t)v_p(t)|v_p(t)| + \Delta d_L(t)v_d(t) \\ & + \Delta b(t) + m\Delta\dot{v}(t) + d_L\Delta v(t) + k_p\Delta x(t) + k_d\Delta v(t)\end{aligned} \tag{20}$$

or rewritten as

$$\Delta\dot{v}(t) = -m^{-1}(\Delta\Psi(t)^T X(t) + (d_L + k_d)\Delta v(t) + k_p\Delta x(t)) \tag{21}$$

where $X(t) = [\dot{v}_d(t); v_p(t)|v_p(t)|; v_d(t); 1]_{4\times 1}$. Note that if the parameter error $\Delta\Psi(t)$ is zero, then (20) becomes the EL closed-loop dynamical system (12).

Define the Lyapunov function candidate as

$$\begin{aligned}W(\Delta x(t), \Delta v(t), \Delta\Psi(t)) = {} & \frac{1}{2}k_p\Delta x(t)^2 + \frac{1}{2}m\Delta v(t)^2 \\ & + \frac{1}{2}\Delta\Psi(t)^T\Gamma^{-1}\Delta\Psi(t).\end{aligned} \tag{22}$$

We can design (22) to have a negative semidefinite time derivative by choosing the parameter update law to be

$$\dot{\hat{\Psi}}(t)_{4\times 1} = \Gamma X(t)\Delta v(t) \tag{23}$$

where $\Gamma_{4\times 4} = \mathrm{diag}[\gamma_i]$, for $i = 1, \ldots, 4$, with $\gamma_i > 0$. The time derivative of (22) is then

$$\dot{W}(\Delta x(t), \Delta v(t), \Delta\Psi(t)) = -(k_d + d_L)\Delta v(t)^2. \tag{24}$$

We conclude the following points.

1) From (22) and (24), $\Delta x(t)$, $\Delta v(t)$, and $\Delta\Psi(t)$ are bounded.
2) Given that $\Delta\Psi(t)$ is bounded and Ψ is a constant, then $\hat{\Psi}(t)$ is bounded as well.
3) Given that $x_d(t)$, $v_d(t)$, and $\dot{v}_d(t)$ are bounded by definition, then from (19) and points 1) and 2), $x_p(t)$ and $v_p(t)$ are bounded.
4) From (21); points 1), 2), and 3); and given that $m \neq 0$, k_p, and k_d are constant, then $\Delta\dot{v}(t)$ is bounded.
5) In consequence, given point 3), $\dot{v}(t)$ is also bounded.
6) Given that $\Delta v(t)$ is bounded from point 1), then $\|\Delta v(t)\| = (\int_0^\infty |\Delta v(t)|^2\, dt)^{1/2}$ exists and is finite. Thus, $\Delta v(t) \in L^2$. In addition, given that $\Delta\dot{v}(t)$ is bounded from point 4), thus we can conclude that $\lim_{t\to\infty}\Delta v(t) = 0$ [50].
7) Given that $\lim_{t\to\infty}\Delta v(t) = 0$, Γ is constant, and $X(t)$ is bounded, then from (23), $\lim_{t\to\infty}\Delta\dot{\Psi}(t) = 0$.

In summary, we have concluded that all signals remain bounded, the velocity tracking error asymptotically goes to zero (the time derivative of the position error asymptotically goes to zero), and the time derivative of the parameter estimates converges asymptotically to zero. However, absent additional arguments, we cannot claim either $\lim_{t\to\infty}\Delta\Psi(t) = 0$ or that $\lim_{t\to\infty}\Delta x(t) = 0$. This controller is an application to underwater vehicles of the general methodology originally reported in [12] and [13].

E. ANL Model-Based Controller

In this section, the ANL model-based controller is presented. The ANL takes the form

$$\begin{aligned}\tau(t) = {} & \hat{m}(t)\dot{v}_d(t) + \hat{d}_Q(t)v_d(t)|v_d(t)| \\ & + \hat{d}_L(t)v_d(t) + \hat{b}(t) + k_p\Delta x(t) + k_d\Delta v(t), \\ & k_p, k_d > 0\end{aligned} \tag{25}$$

where $\hat{m}(t)$, $\hat{d}_Q(t)$, $\hat{d}_L(t)$, and $\hat{b}(t)$ are estimates of the scalar plant parameter values; $\tau(t)$ is the controller output; and k_p and k_d are PD scalar error feedback gains. The plant parameter error coordinates are defined in (19) and the state error coordinates are defined in (9). Substituting (25) into (3), the resulting closed-loop dynamical system is

$$\begin{aligned}0 = {} & \Delta m(t)\dot{v}_d(t) + \Delta d_Q(t)v_d(t)|v_d(t)| + \Delta d_L(t)v_d(t) \\ & + \Delta b(t) + m\Delta\dot{v}(t) + d_Q(v_d(t)|v_d(t)| - v_p(t)|v_p(t)|) \\ & + d_L\Delta v(t) + k_p\Delta x(t) + k_d\Delta v(t)\end{aligned} \tag{26}$$

which can be rewritten as

$$\begin{aligned}\Delta\dot{v}(t) = {} & -m^{-1}(\Delta\Psi(t)^T X(t) + d_Q(v_d(t)|v_d(t)| \\ & - v_p(t)|v_p(t)|) + (d_L + k_d)\Delta v(t) + k_p\Delta x(t))\end{aligned} \tag{27}$$

where $X(t) = [\dot{v}_d(t); v_d(t)|v_d(t)|; v_d(t); 1]_{4\times 1}$. Note that if the parameter error is zero, $\Delta\Psi(t) = 0$, then (26) becomes the NL closed-loop dynamical system (14).

Consider the Lyapunov function candidate

$$\begin{aligned}& W(\Delta x(t), \Delta v(t), \Delta\Psi(t)) \\ & \quad = \frac{1}{2}k_p\Delta x(t)^2 + \frac{1}{2}m\Delta v(t)^2 + \frac{1}{2}\Delta\Psi(t)^T\Gamma^{-1}\Delta\Psi(t).\end{aligned} \tag{28}$$

We can design (29) to have a negative semidefinite time derivative by choosing the parameter update law to be

$$\dot{\hat{\Psi}}(t)_{4\times 1} = \Gamma X(t)\Delta v(t) \tag{29}$$

where $\Gamma_{4\times 4} = \mathrm{diag}[\gamma_i]$, for $i = 1 \cdots 4$, with $\gamma_i > 0$. The resulting time derivative of (22) is

$$\begin{aligned}\dot{W}(\Delta x(t), \Delta v(t), \Delta\Psi(t)) = {} & -(k_d + d_L)\Delta v(t)^2 \\ & - d_Q(v_d(t)|v_d(t)| - v_p(t)|v_p(t)|)\Delta v(t).\end{aligned} \tag{30}$$

The first term in (30) is negative definite in $\Delta v(t)$ and, following the same argument made in Section III-C, we can conclude that (30) is negative semidefinite. We conclude the following points.

1) From (29) and (30), $\Delta x(t)$, $\Delta v(t)$, and $\Delta\Psi(t)$ are bounded.
2) Given that $\Delta\Psi(t)$ is bounded and Ψ is a constant, then $\hat{\Psi}(t)$ is bounded as well.

TABLE IV
JHUROV SIMULATION TRAJECTORIES AND GAINS

DOF	Magnitude	Frequency	Period	k_p	k_d	γ_1	γ_2	γ_3	γ_4	ϵ
x_1	0.5 m	0.3925 rad/s	16 s	500	200	5000	1e5	0	0.1	1

3) Given that $x_d(t)$, $v_d(t)$, and $\dot{v}_d(t)$ are defined to be bounded, then $x_p(t)$ and $v_p(t)$ are bounded.
4) From (27) and points 1), 2), and 3), and given that $m \neq 0$, k_p, and k_d are constant, then $\Delta\dot{v}(t)$ is bounded.
5) In consequence, given point 3), $\dot{v}(t)$ is also bounded.
6) From (30) and that $d_Q(v_d(t)|v_d(t)| - v_p(t)|v_p(t)|)\Delta v(t) \geq 0$, as argued earlier, we get $\Delta v(t)^2 \leq -W(\Delta v(t), \Delta x(t))/(d_L + k_d)$.
7) Given that $\Delta v(t)$ is bounded from point 1), then $\|\Delta v(t)\| = (\int_0^\infty |\Delta v(t)|^2\, dt)^{1/2}$ exists and is finite. Thus, $\Delta v(t) \in L^2$. In addition, given that $\Delta\dot{v}(t)$ is bounded from point 4), we can thus conclude $\lim_{t\to\infty} \Delta v(t) = 0$ [50].
8) Given point 7), Γ is constant and $X(t)$ is bounded. Then, from (29), we conclude $\lim_{t\to\infty} \Delta\dot{\hat{\Psi}}(t) = 0$.

In summary, we have concluded that all signals remain bounded and that both the velocity tracking error and the time derivative of the parameter estimates converge asymptotically to zero. However, absent additional arguments, we cannot claim either $\lim_{t\to\infty} \Delta\Psi(t) = 0$ or that $\lim_{t\to\infty} \Delta x(t) = 0$. This approach is an application to underwater vehicles of the general methodology originally reported in [52], [53] and [62].

F. ϵANL Model-Based Controller

Although the ANL controller was shown to be stable, bounded, and to provide asymptotically exact velocity tracking, it does not guarantee asymptotically exact position tracking. This apparent defect can be corrected with a modification of the parameter update law. The idea is to introduce a small cross term of the form $\epsilon m\Delta x(t)\Delta v(t)$; $\epsilon > 0$, to the Lyapunov function. If ϵ is sufficiently small, the Lyapunov function remains positive definite and radially unbounded and its time derivative is locally negative definite. This local stability result was first reported independently in [6], [39], and [61]. A globally stable variation was reported in [62]. Applying this approach to the present plant, (3), the control law (25) remains unchanged, resulting in the closed-loop dynamical system (26).

Consider the Lyapunov function candidate

$$W(\Delta x(t), \Delta v(t), \Delta\Psi(t)) = \frac{1}{2}k_p\Delta x(t)^2 + \frac{1}{2}m\Delta v(t)^2 + \epsilon m\Delta x(t)\Delta v(t) + \frac{1}{2}\Delta\Psi(t)^T\Gamma^{-1}\Delta\Psi(t). \quad (31)$$

For ϵ sufficiently small, this function is positive definite and radially unbounded. Choosing the new parameter update law

$$\dot{\hat{\Psi}}(t) = \Gamma X(t)(\Delta v(t) + \epsilon\Delta x(t)) \quad (32)$$

where

$$X(t) = [\dot{v}_d(t), v_d(t)|v_d(t)|, v_d(t), 1]_{4\times 1}, \quad \epsilon > 0, \gamma_i \geq 0, \quad \Gamma_{4\times 4} = \mathrm{diag}[\gamma_i], i = 1, \ldots, 4 \quad (33)$$

the time derivative of (31) is

$$\dot{W}(\Delta x(t), \Delta v(t), \Delta\Psi(t)) = -(k_d + d_L - \epsilon m)\Delta v(t)^2 - d_Q(v_d(t)|v_d(t)| - v_p(t)|v_p(t)|)\Delta v(t) - \epsilon k_p\Delta x(t)^2 - \epsilon(d_Q(v_d(t)|v_d(t)| - v_p(t)|v_p(t)|) + (k_d + d_L)\Delta v(t))\Delta x(t).$$

As reported in [6], [39], [61], and [62], the time derivative of this Lyapunov function is locally negative definite. Note that, in the case of $\epsilon = 0$, the ϵANL is identical to the ANL controller.

G. Numerical Simulation of Controller Performance

An advantage to having an experimentally validated dynamical plant model of the JHUROV is that we can simulate the performance of the model-based controllers prior to implementing them experimentally. Simulations were run in the x_1, x_2, x_3, and x_4 DOF, where the vehicle was commanded to track a trajectory under closed-loop control. The model parameters presented in Table III were used to simulate the JHUROV's dynamical behavior. We present the results from the x_1 DOF here. The simulations correspond directly to experimental results reported in Section V-A. Table IV lists the trajectories and gains used in the simulations; all simulations were run with identical initial conditions to the corresponding experiments in Section V-A.

In the case of the PD controller in Fig. 1, the simulations show that both the position and velocity tracking errors remain bounded. As predicted by theory, we see in Fig. 2 that both the velocity and position tracking error go to zero for the EL controller. Similarly for the NL controller, Fig. 3 supports the theory in that both error signals remain bounded and the velocity tracking error goes to zero. In addition to what was predicted by theory, we see that the position tracking error goes to zero as well.

Figs. 4 and 5 demonstrate the simulated performance of the AEL and ANL controllers. In the case of the AEL controller, we see that all signals remain bounded, the velocity error goes to zero and as seen in Fig. 7, and the adaptive parameters converge to a value as expected. Similarly for the ANL controller, all signals remain bounded, the velocity error goes to zero and as seen in Fig. 8, and the adaptive parameters converge to a value as expected. The position tracking error does not go to zero for either of the AEL or ANL controllers in simulation. In looking at the simulation results for the ϵANL (Figs. 6 and 9) we see that the adaptive parameters converge to a final value and the velocity tracking error goes to zero. In addition, the position tracking error goes to zero.

We have adopted a position and velocity error norm to quantitatively compare the performance of this family of controllers. The position error norm reported for each DOF i was calculated as $X_{\mathrm{err}_i} = \mathrm{mean}(|x_{d_i} - x_{p_i}|)$ where x_{d_i} and x_{p_i} are the desired/reference and simulated position of the

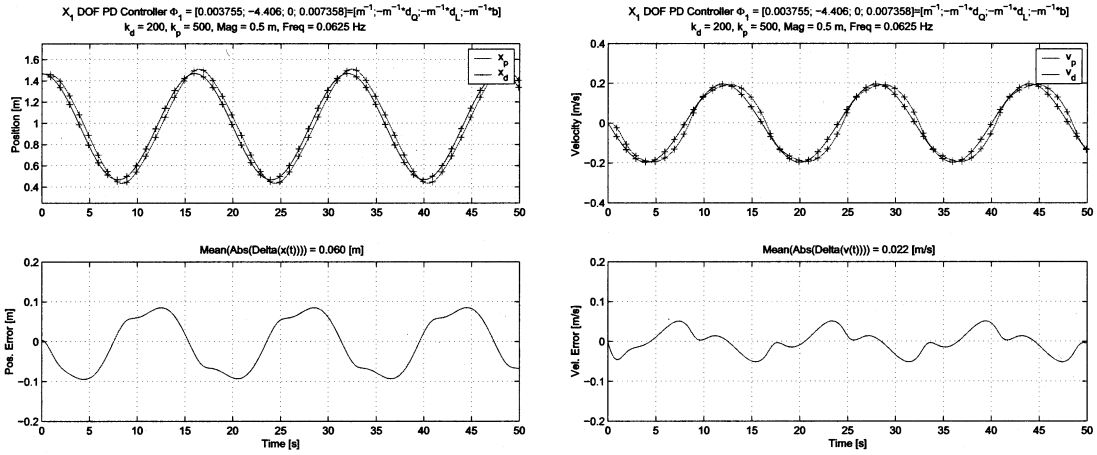

Fig. 1. Simulation of PD controller in x_1 DOF. Top: Plot of simulated vehicle position x_p versus desired position x_d (left) simulated vehicle velocity v_p versus (right) desired velocity v_d. Bottom: Plot of (left) position tracking error $\Delta x(t)$ and (right) velocity tracking error $\Delta v(t)$. The reference trajectory is a 1/16-Hz sinusoid, $x_d = 0.5\ \cos(2 * \pi * (1/16) * t)$ [m].

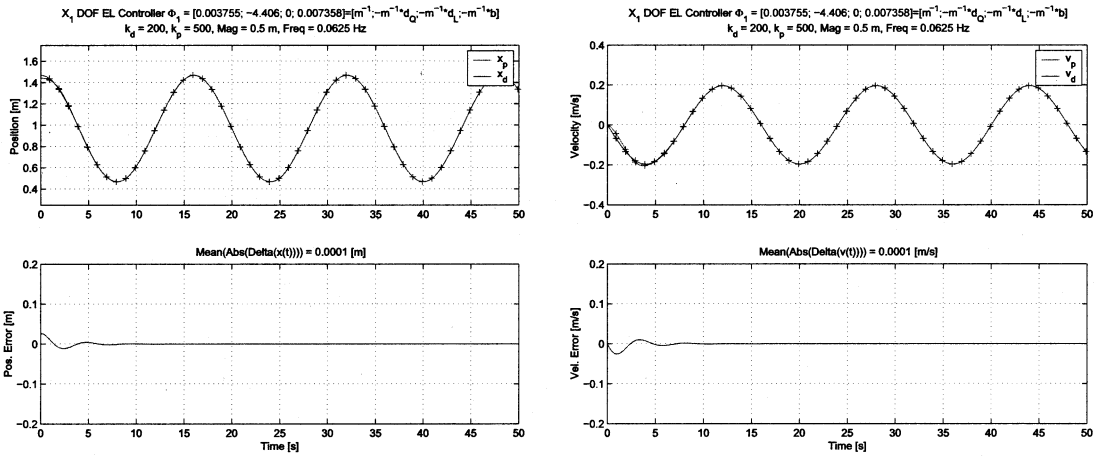

Fig. 2. Simulation of EL controller in x_1 DOF. Top: (left) plot of simulated vehicle position x_p versus desired position x_d, (right) simulated vehicle velocity v_p versus desired velocity v_d. Bottom: (left) plot of position tracking error $\Delta x(t)$ and (right) velocity tracking error $\Delta v(t)$. The reference trajectory is a 1/16-Hz sinusoid, $x_d = 0.5\ \cos(2 * \pi * (1/16) * t)$ [m].

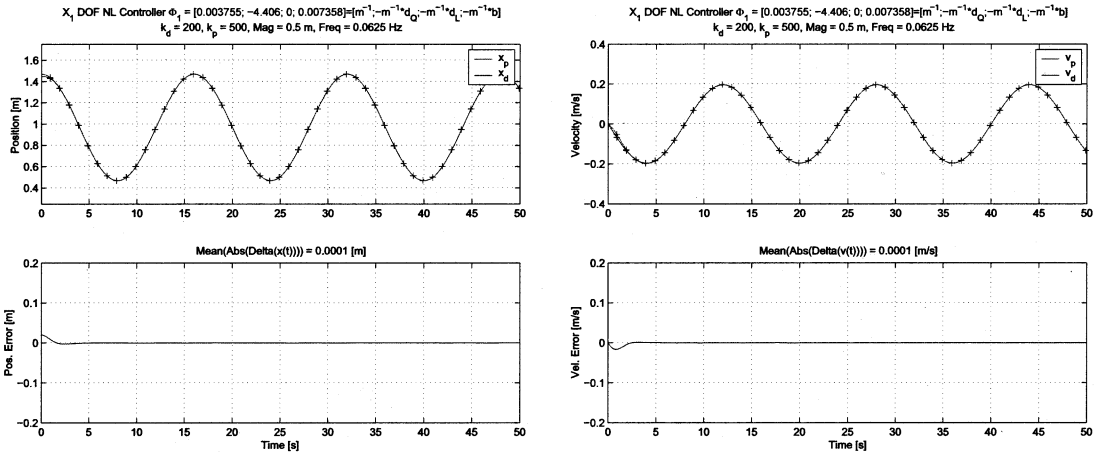

Fig. 3. Simulation of NL controller in x_1 DOF. Top: (left) plot of simulated vehicle position x_p versus desired position x_d, (right) simulated vehicle velocity v_p versus desired velocity v_d . Bottom: (left) plot of position tracking error $\Delta x(t)$ and (right) velocity tracking error $\Delta v(t)$. The reference trajectory is a 1/16-Hz sinusoid, $x_d = 0.5\ \cos(2 * \pi * (1/16) * t)$ [m].

JHUROV in DOF i. The velocity error norm was calculated as $V_{\mathrm{err}_i} = \mathrm{mean}(|v_{d_i} - v_{p_i}|)$, where v_{d_i} and v_{p_i} are the desired/reference and simulated velocity of the JHUROV in DOF i. Fig. 10 displays a bar chart containing both the position and velocity tracking error for each controller in the x_1 DOF for the reference trajectories listed in Table IV. The

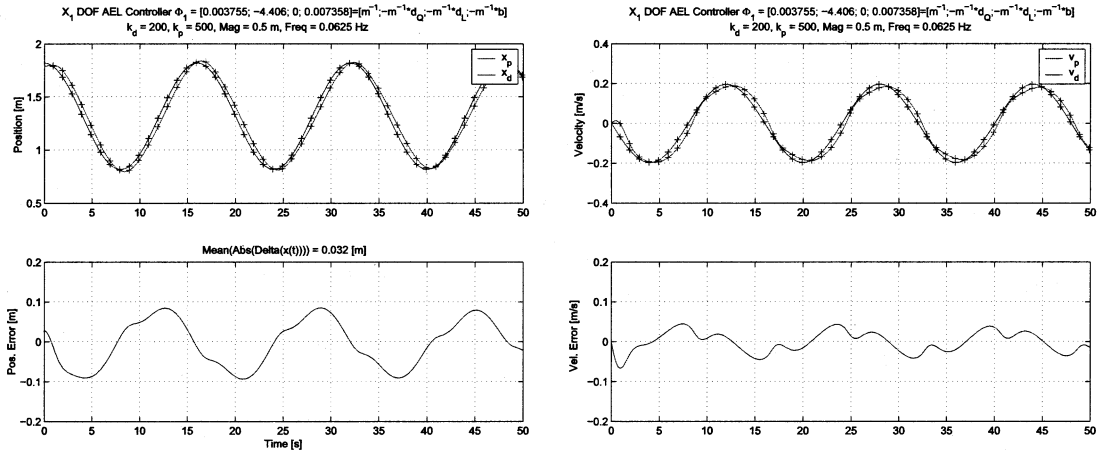

Fig. 4. Simulation of AEL controller in x_1 DOF. Top: (left) plot of simulated vehicle position x_p versus desired position x_d, (right) simulated vehicle velocity v_p versus desired velocity v_d. Bottom: (left) plot of position tracking error $\Delta x(t)$ and (right) velocity tracking error $\Delta v(t)$. The reference trajectory is a 1/16-Hz sinusoid, $x_d = 0.5\ \cos(2 * \pi * (1/16) * t)$ [m].

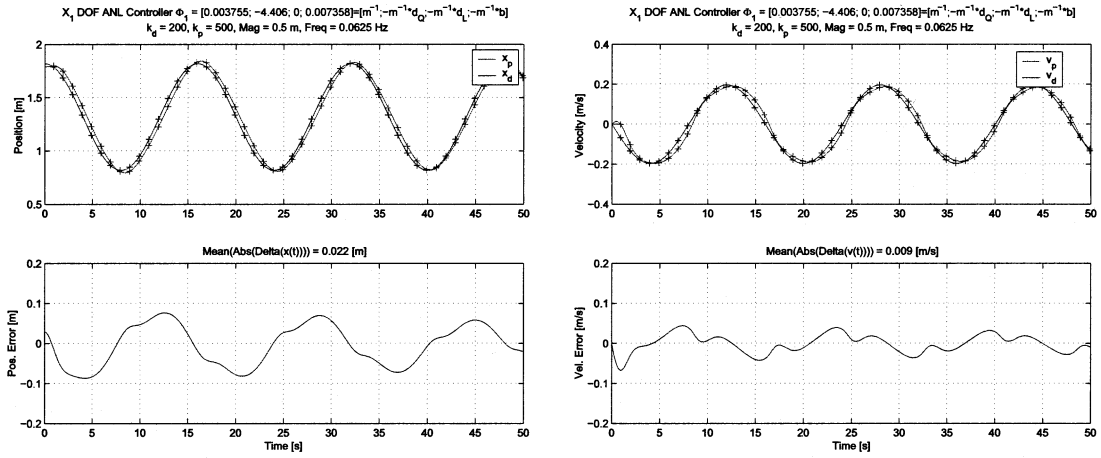

Fig. 5. Simulation of ANL controller in x_1 DOF. Top: Plot of simulated vehicle position x_p versus desired position x_d (Left), simulated vehicle velocity v_p versus desired velocity v_d (Right). Bottom: Plot of position tracking error $\Delta x(t)$ (Left) and velocity tracking error $\Delta v(t)$ (Right). The reference trajectory is a 1/16-Hz sinusoid, $x_d = 0.5\ \cos(2 * \pi * (1/16) * t)$ [m].

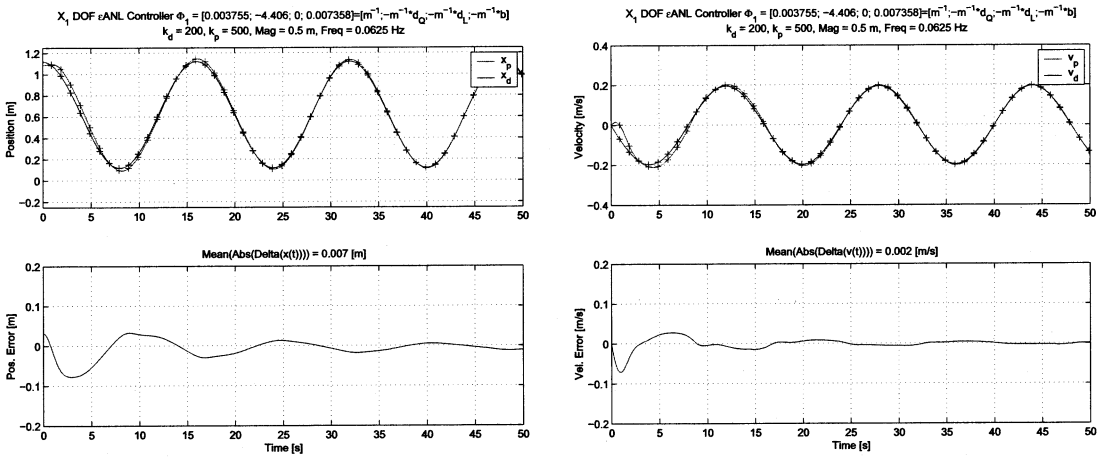

Fig. 6. Simulation of ϵANL controller in x_1 DOF. Top: (left) plot of simulated vehicle position x_p versus desired position x_d, (right) simulated vehicle velocity v_p versus desired velocity v_d. Bottom: (left) plot of position tracking error $\Delta x(t)$ and (right) velocity tracking error $\Delta v(t)$. The reference trajectory is a 1/16 Hz sinusoid, $x_d = 0.5\ \cos(2 * \pi * (1/16) * t)$ [m]. $\epsilon = 1.0$.

corresponding plots of the simulated vehicle position and velocity and the reference position and velocity versus time are presented in Figs. 1–9. Some plots are shortened with respect to time (y-axis) to zoom in for detail.

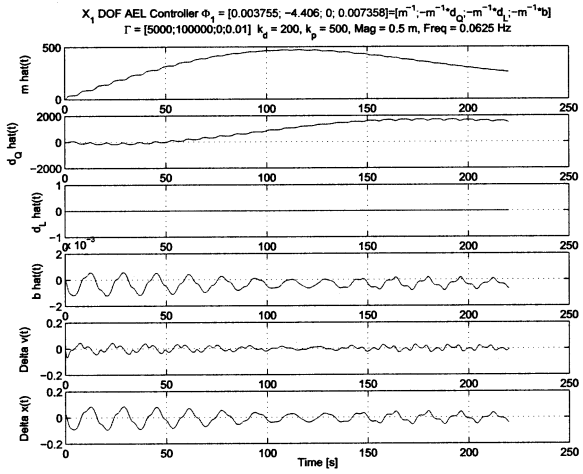

Fig. 7. Simulation of AEL controller in x_1 DOF. Top to bottom: Plot of adaptive parameters $\hat{m}_1(t)$, $\hat{d}_{Q_1}(t)$, $\hat{d}_{L_1}(t)$, $\hat{b}_1(t)$, and $\Delta v(t)$, and $\Delta x(t)$ versus time. The reference trajectory is a 1/16 Hz sinusoid, $x_d = 0.5\ \cos(2 * \pi * (1/16) * t)$ [m].

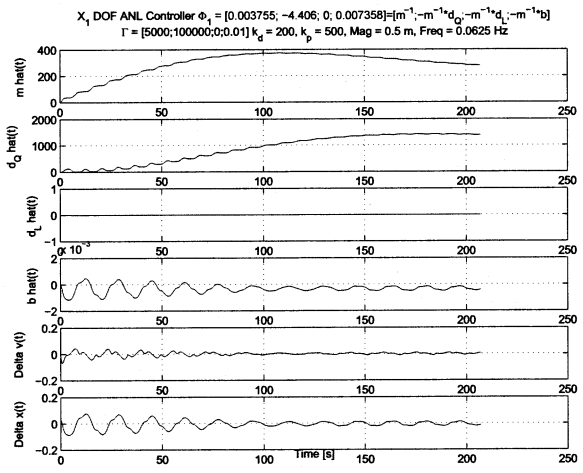

Fig. 8. Simulation of ANL controller in x_1 DOF. Top to bottom: Plot of adaptive parameters $\hat{m}_1(t)$, $\hat{d}_{Q_1}(t)$, $\hat{d}_{L_1}(t)$, $\hat{b}_1(t)$, and $\Delta v(t)$ and $\Delta x(t)$ versus time. The reference trajectory is a 1/16 Hz sinusoid, $x_d = 0.5\ \cos(2 * \pi * (1/16) * t)$ [m].

IV. Experimental Setup

The JHUROV, shown in Fig. 11, is a tethered remotely operated underwater robot. The JHUROV is powered by an isolated 10-kW dc power supply. The dry mass of the vehicle is 140 kg and its dimensions are 1.5 m long × 1 m wide × 0.6 m high. The position and heading of the vehicle are actively controlled and the vehicle is passively stable in roll and pitch. Actuation is provided by five dc brushless electric thrusters. A complete description of the JHUROV is reported in [54] and [55].

The JHUROV is equipped for full six-DOF position measurement. For this set of experiments, XYZ position was measured using a 300-kHz sonic high accuracy ranging and positioning system (SHARPS) time-of-flight acoustic hardwired transponder system. Depth was instrumented via a Paroscientific 8DP-700-1 Digiquartz depth sensor, sampled at 8 Hz. A KVH Azimuth Digital Gyro Compass (ADGC) measured the vehicle's roll and pitch. Heading was measured using a prototype Litton LN200 IMU. The vehicle's entire sensor suite is listed in Table V.

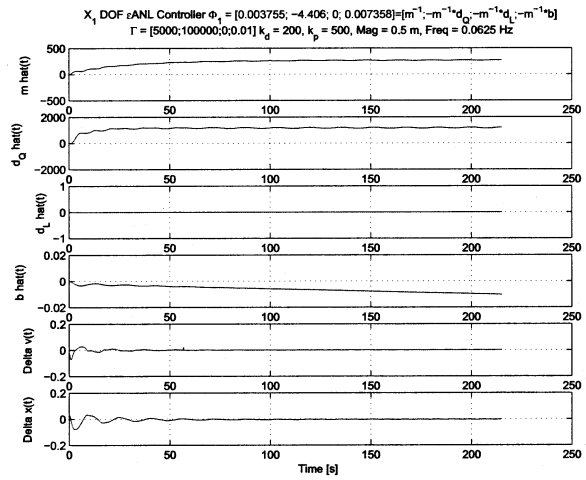

Fig. 9. Simulation of ϵANL controller in x_1 DOF. Top to bottom: Plot of adaptive parameters $\hat{m}_1(t)$, $\hat{d}_{Q_1}(t)$, $\hat{d}_{L_1}(t)$, $\hat{b}_1(t)$, and $\Delta v(t)$ and $\Delta x(t)$ versus time. The reference trajectory is a 1/16 Hz sinusoid, $x_d = 0.5 \cos(2 * \pi * (1/16) * t)$ [m].

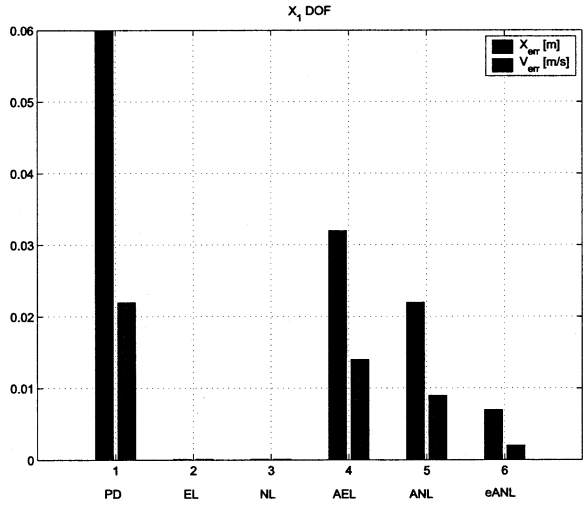

Fig. 10. Plot of simulation tracking error for the PD, EL, NL, AEL, ANL, and ϵANL controllers in the x_1 DOF. The reference trajectory is a 1/16 Hz sinusoid, $x_d(t) = 0.5\ \cos(2 * \pi * (1/16) * t)$ [m]. $X_{\mathrm{err}_1} = \mathrm{mean}(|x_{d_1} - x_{p_1}|)$ [m], $V_{\mathrm{err}_1} = \mathrm{mean}(|v_{d_1} - v_{p_1}|)$ [m/s].

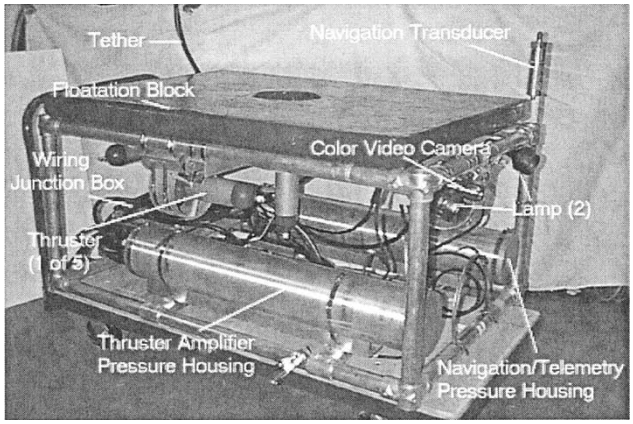

Fig. 11. The JHUROV, a 140-kg 1000-m vehicle.

TABLE V
INSTRUMENTATION

Variable	Sensor	Precision	Update Rate
XYZ Position	300 kHz SHARPS Acoustic Transponder System	5 mm	10 Hz
Depth	Paroscientific	10ppm FS (7mm)	8 Hz
Heading	Litton LN200 IMU Gyro (USNA)	0.01 deg.	20 Hz
Roll and Pitch	KVH ADGC	0.1 deg.	20 Hz
Heading	KVH ADGC	1 deg	20 Hz

Open-loop experiments were conducted in the x_1, x_2, x_3, and x_4 DOF to identify the plant model parameters. Multiple trials in each DOF were conducted with sinusoidal thrust profiles of varying peak magnitude and frequency. A detailed description of the model identification procedure can be found in [55] and [57].

A static thrust model was used for these experiments to model the thrust produced by each thruster—i.e., the thrust τ produced is assumed to be proportional to the current commanded i_c, as in $i_c(t) = k_t^{-1}\tau(t)$. Current was controlled using current mode amplifiers. The authors are aware of more advanced thruster models [7], [34] that are more precise; however, they require a dynamical thruster characterization not available at the time of these experiments.

Closed-loop experiments were conducted in the x_1, x_2, x_3, and x_4 DOF to test the controllers. Multiple trials were conducted using each controller tracking sinusoidal position and velocity reference trajectories of varying peak magnitude and frequency. The velocity trajectory is the time derivative of the position trajectory. In this paper, wherever position is specified, it is in inertial world coordinates, whereas velocity is in body coordinates. Whenever specifications such as peak magnitude and frequency are given regarding reference trajectories, they are for a position reference trajectory.

A. Navigation System Precision

Determining the dynamical behavior of the JHUROV in the x_1, x_2, x_3, and x_4 DOF requires the measurement of the JHUROV's position in all six DOF. Measuring depth, heading, pitch, and roll with a high degree of precision is fairly common in underwater vehicles; measuring the X–Y (x_1 and x_2) position is not. What made this work possible is the use of a 300-kHz SHARPS acoustic time of flight system. To experimentally determine the precision and resolution of this position measuring system, an experimental trial was run in which the JHUROV was left sitting completely motionless at the bottom of the test tank. The results are shown in Fig. 12.

Analyzing the data, we see that we are able to achieve a resolution in the *millimeter* range in the x_1-x_2 plane. The standard deviations were submillimeter in the x_1 direction and around 2 mm in the x_2 direction. The difference between these two numbers is a consequence of the particular transponder layout, range, and depth of the vehicle. The specifications for the depth sensor indicate an accuracy of 0.01% of full scale. With an update rate of 8 Hz and maximum range of 700 m, the sensor had a precision of approximately 0.007 m (10 ppm). The raw depth sensor values were filtered using a second-order 1-Hz low-pass Butterworth filter. The inertial measurement unit (IMU) heading had a precision on the order of hundredths of a degree. The gyro exhibited a systematic drift and the drift was compensated for by resetting the gyro position to the heading of the baseline at regular intervals.

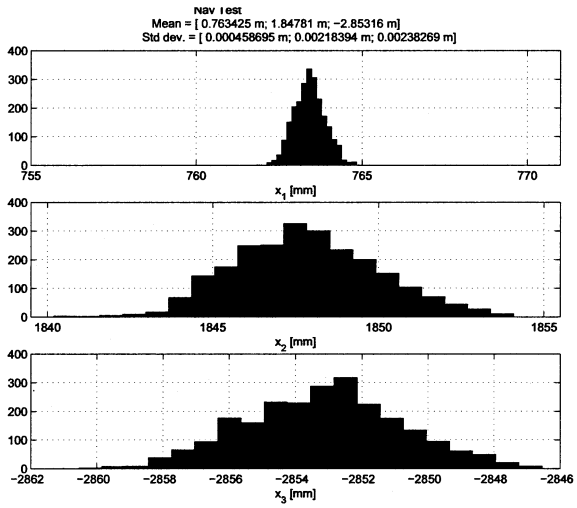

Fig. 12. Histogram of JHUROV x_1, x_2, and x_3 position during navigational system precision test.

V. EXPERIMENTAL RESULTS

This section reports a comparative experimental evaluation of the tracking performance of the EL, NL, AEL, ANL, ϵANL, and PD controllers. First, a direct comparison between PD and the fixed model-based controllers is reported. The EL is directly compared to NL and a direct comparison between the fixed and adaptive model-based controller is presented. We investigate the effect of model accuracy on the model-based controllers. The effects of different trajectories on controller performance is reported. The effect of various PD gains on the fixed controllers and adaptation gains on the adaptive controllers is examined. Finally, the effect of thruster saturation on controller performance is reported.

A. Comparative Controller Performance

This section reports a direct comparison of the performance of the EL, NL, and PD controllers while tracking a sinusoidal trajectory of the same peak magnitude and frequency. This is followed by a comparison of the performance of the adaptive model-based controllers (AEL, ANL, and ϵANL) to the fixed model-based controllers (EL and NL) tracking the same trajectory.

1) PD Versus Model-Based Control: The PD, EL, and NL controllers were implemented to track a sinusoidal reference trajectory of the same peak magnitude and frequency. For each

TABLE VI
PD VERSUS MODEL-BASED COMPARISON

DOF	Magnitude	Frequency	Period	k_p	k_d
x_1	0.5 m	0.3925 rad/s	16 Seconds	500	200
x_2	0.25 m	0.3925 rad/s	16 Seconds	500	200
x_3	0.2 m	0.524 rad/s	12 Seconds	600	800
x_4	45 degrees	0.3925 rad/s	16 Seconds	250	100

DOF, each controller used the same set of PD gains, k_p and k_d, listed in Table VI.

Examining Fig. 13, it is clear that the NL controller outperforms the basic PD controller in position trajectory tracking. It is also clear that graphical plots such as Fig. 13 are more of a qualitative approach to evaluating controller performance. As a result, we have adopted a position and velocity error norm to quantitatively compare the performance of this family of controllers across a wide range of operating conditions. The position error norm reported for each DOF i was calculated as $X_{\mathrm{err}_i} = \mathrm{mean}(|x_{d_i} - x_{p_i}|)$ where x_{d_i} and x_{p_i} are the desired/reference and actual logged position of the JHUROV in DOF i. The velocity error norm was calculated as $V_{\mathrm{err}_i} = \mathrm{mean}(|v_{d_i} - v_{p_i}|)$, where v_{d_i} and v_{p_i} are the desired/reference and actual logged velocity of the JHUROV in DOF i. Bar charts displaying both the position and velocity tracking error for each controller in each DOF can be seen in Figs. 14–17 for the reference trajectories listed in Table VI.

Based on the error metric reported, it is clear that: 1) the NL controller performs as well or better than the EL controller in each DOF and 2) both fixed model-based controllers outperform the basic PD controller tracking the trajectory.

2) Adaptive versus Fixed Model-Based Control: The adaptive model-based controllers were run on the same trajectories as the nonadaptive controllers using the same sets of PD gains, listed in Table VI. The adaptive controllers have the added complexity of setting the adaptation gains γ_i. For the purpose of this direct comparison, the adaptation gains were the same for the AEL, ANL, and the ϵANL controllers in each DOF. The adaptation gains can be found in Table VII, which were chosen as a result of numerical simulations run prior to the experiments. Comparing the performance of the AEL, ANL, and ϵANL controllers, the ϵANL controller did the best job tracking the position trajectory in all but the x_4 DOF. The ϵANL controller also tracked the velocity reference trajectory the best in the x_1 and x_2 DOF. The ANL controller performed the best of the adaptive controllers in tracking the velocity in the x_3 and x_4 DOF.

If we compare the performance of the AEL to the fixed model-based controllers, we see that it did a worse job in tracking both the position and velocity trajectories than did the fixed model-based controllers. Similarly, the ANL did not perform as well as either of the fixed model-based controllers. However, when compared directly to the basic PD controller, we see that the ANL outperformed the basic PD controller in the x_1, x_3, and x_4 DOF and performed comparably to the basic PD controller in the x_2 DOF. The AEL also outperformed the basic PD controller in the x_3 and x_4 DOF, but fared worse when used to track a position and velocity trajectory in the x_1 and x_2 DOF. The ϵANL controller performed comparably or better than the fixed model-based controllers in the x_1 and x_2 DOF and clearly outperformed the basic PD controller in all but the x_4 DOF.

We conclude that the model-based controllers (EL, NL, AEL, ANL, and ϵANL) as a group generally perform as well or better then the basic PD controller in trajectory tracking. In comparing the fixed with the adaptive model-based controllers, we conclude that if the "right" adaptation law is chosen, the adaptive model-based controllers may provide superior trajectory tracking performance compared to the fixed model-based controllers. By this we mean that while the AEL and ANL controllers consistently performed worse than the NL and EL fixed model-based controllers. The ϵANL controller in the x_1 and x_2 DOF performed as well or better then the EL and NL fixed model-based controllers.

B. Effect of Different Trajectories on Controller Performance

How is the controller's tracking performance effected by different reference trajectories? Fig. 14 presents the results for one particular trajectory. In this section, we present results from a different trajectory in the x_1 DOF and discuss what effect the peak magnitude and frequency of the trajectory had on controller performance. Fig. 18 contains bar charts of the position and velocity tracking errors for the PD, EL, NL, AEL, ANL, and ϵANL controllers. The peak magnitude and frequency of the reference trajectory is listed in Table VIII. Each controller was run using the same identical PD and adaptation gains as used for the data reported in Tables VI and VII in Section V-A, with the exception of the ϵANL controller. Unfortunately, no data was available for the ϵANL controller on this trajectory using the same adaptation gains as used by the AEL and ANL controllers. The only difference is the value for the γ_4 gains, as seen in Table IX.

Comparing the results in Fig. 18 to those in Fig. 14, we see that controller tracking performance is not significantly effected by the different trajectories. Corroborating the results reported in Section V-A, the NL controller outperformed the EL fixed model-based controller and both the EL and NL fixed model-based controllers performed as well as or better then the PD controller. Similarly, both the AEL and ANL adaptive model-based controllers performed as well as or better than the PD controller tracking the reference trajectory. The AEL and ANL controller performance was still slightly worse than the fixed model-based controllers.

While the trajectory tracking performance is not significantly effected by the different trajectories, the convergence of the adaptive parameter estimates in the adaptive model-based controllers is noticeably effected. This can be seen in Fig. 19, where the adaptive parameter estimates converged quicker while tracking the trajectory of peak magnitude 0.25 m and frequency 0.785 rad/s.

We conclude that the effect of different trajectories on controller tracking performance is minimal when the trajectories are within the thruster and sensor limits. The overall performance of the controllers tracking one trajectory is not drastically different than the tracking performance on another trajectory. The one effect seen is that adaptive parameter estimates of adaptive controllers may converge more quickly on certain trajectories;

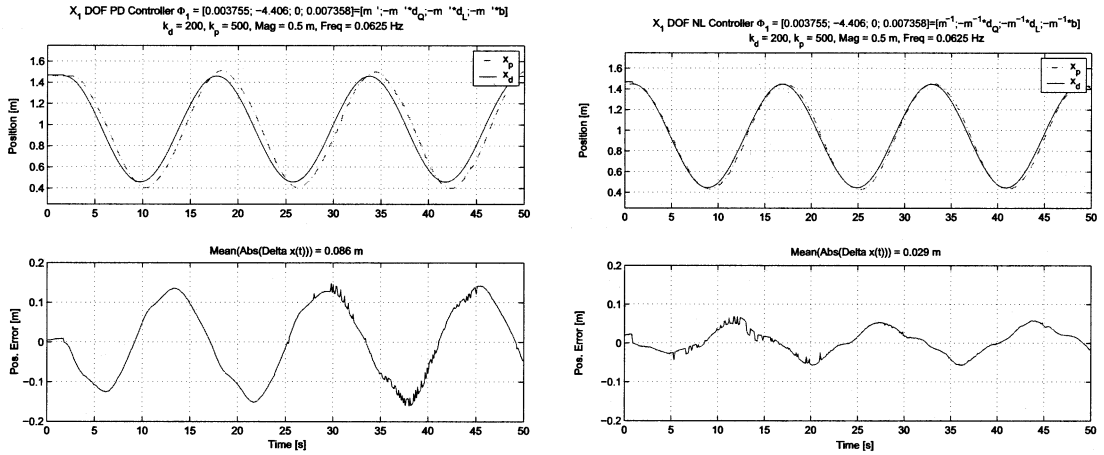

Fig. 13. Top: Plot of actual vehicle position (X_p) versus desired reference trajectory (X_d) for (left) the PD controller and (right) NL controller in the x_1 DOF. Bottom: Plot of position tracking error for the (left) PD controller and (right) NL controller in the x_1 DOF. The reference trajectory is a 1/16 Hz sinusoid, $x_d(t) = 0.5\cos(2 * \pi * (1/16) * t)$ [m].

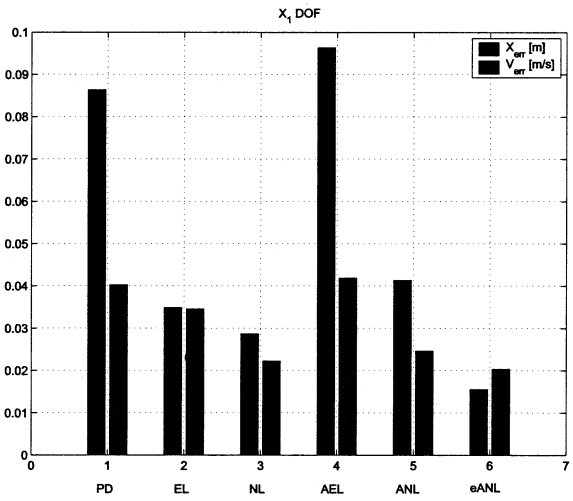

Fig. 14. Plot of tracking error for the PD, EL, NL, AEL, ANL, and ϵANL controllers in the x_1 DOF. The reference trajectory is a 1/16 Hz sinusoid, $x_d(t) = 0.5\cos(2 * \pi * (1/16) * t)$ [m]. $X_{\mathrm{err}_1} = \mathrm{mean}(|x_{d_1} - x_{p_1}|)$ [m], $V_{\mathrm{err}_1} = \mathrm{mean}(|v_{d_1} - v_{p_1}|)$ [m/s].

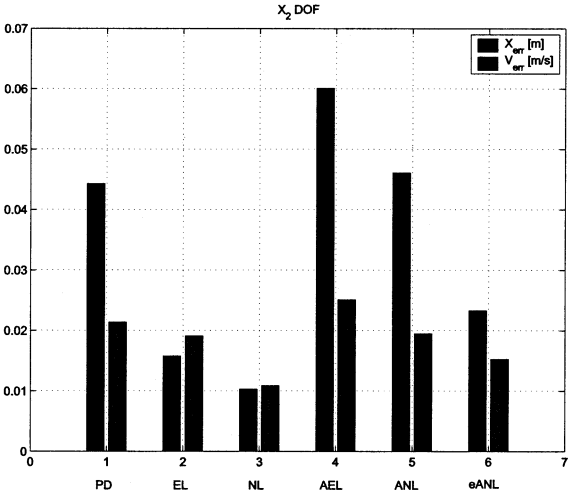

Fig. 15. Plot of tracking error for the PD, EL, NL, AEL, ANL, and ϵANL controllers in the x_2 DOF. The reference trajectory is a 1/16-Hz sinusoid, $x_d(t) = 0.25\cos(2 * \pi * (1/16) * t)$ [m]. $X_{\mathrm{err}_2} = \mathrm{mean}(|x_{d_2} - x_{p_2}|)$ [m], $V_{\mathrm{err}_2} = \mathrm{mean}(|v_{d_2} - v_{p_2}|)$ [m/s].

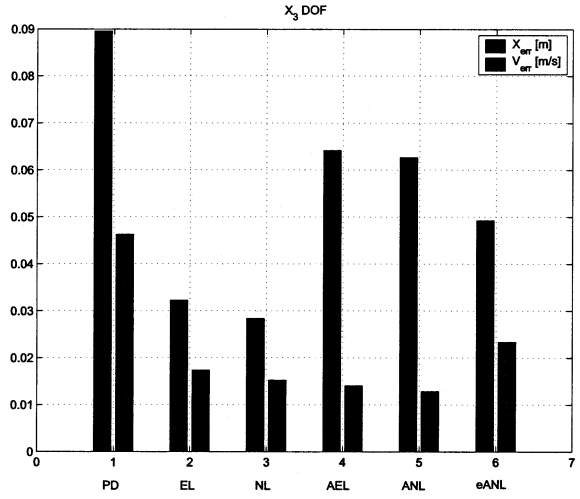

Fig. 16. Plot of tracking error for the PD, EL, NL, AEL, ANL, and ϵANL controllers in the x_3 DOF. The reference trajectory is a 1/12-Hz sinusoid, $x_d(t) = 0.2\cos(2 * \pi * (1/12) * t)$ [m]. $X_{\mathrm{err}_3} = \mathrm{mean}(|x_{d_3} - x_{p_3}|)$ [m], $V_{\mathrm{err}_3} = \mathrm{mean}(|v_{d_3} - v_{p_3}|)$ [m/s].

however, this did not appear to effect trajectory tracking performance significantly.

C. Effect of "Bad" Model Parameters

How do "inaccurate" model parameters effect the performance of the model-based controllers? We have shown in Section V-A that the model-based controllers perform better than a basic PD controlled when designed with model parameters accurately identified. To demonstrate what happens when a model-based controller is designed based on "inaccurate" model parameters, the JHUROV was commanded to track a position and velocity reference trajectory using the NL model-based controller using both "accurate" and "inaccurate" model parameter values. The results were directly compared and the PD and EL controllers were also run for comparison. This test was run in the x_4 DOF. The PD gains were the same for all the controllers ($k_p = 250$, $k_d = 100$) and the trajectory tracked was of the same peak magnitude (0.436 rad) and frequency (0.785 rad/s). As seen by the results in

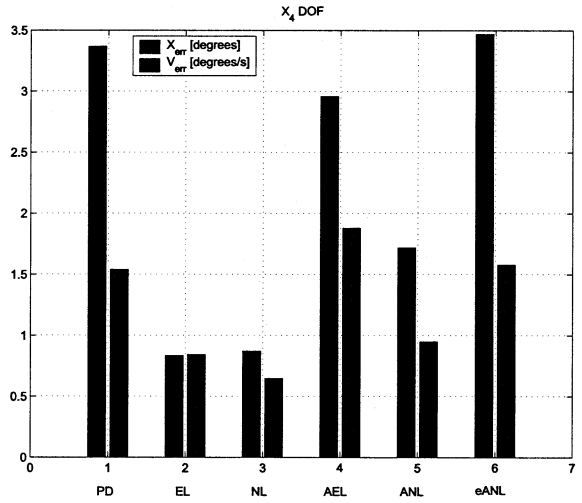

Fig. 17. Plot of tracking error for the PD, EL, NL, AEL, ANL, and ϵANL controllers in the x_4 DOF. The reference trajectory is a 1/16-Hz sinusoid, $x_d(t) = 45\ \cos(2 * \pi * (1/16) * t)$[deg]. $X_{\mathrm{err}_4} = \mathrm{mean}(|x_{d_4} - x_{p_4}|)$[deg], $V_{\mathrm{err}_4} = \mathrm{mean}(|v_{d_4} - v_{p_4}|)$[deg/$s$].

TABLE VII
ADAPTATION GAINS

DOF	γ_1	γ_2	γ_3	γ_4
x_1	5000	100000	0	0.01
x_2	5000	100000	0	0.01
x_3	50000	5000000	0	1
x_4	500	50000	0	1

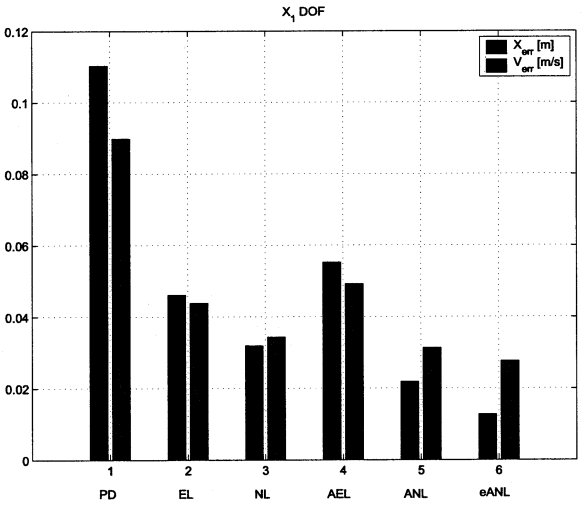

Fig. 18. Plot of tracking error for the PD, EL, NL, AEL, ANL, and ϵANL controllers in the x_1 DOF. Reference trajectory is $x_d(t) = 0.25\cos(2 * \pi * (1/8) * t)$ [m]. $k_p = 500$ and $k_d = 200$. $X_{\mathrm{err}_1} = \mathrm{mean}(|x_{d_1} - x_{p_1}|)$ [m], $V_{\mathrm{err}_1} = \mathrm{mean}(|v_{d_1} - v_{p_1}|)$ [m/s].

Table X, a model-based controller is not necessarily better than a nonmodel-based controller. Clearly, the accuracy of the model parameters themselves play an important role in the performance of the controller. While the "inaccurate" parameter values used were roughly a factor of two different than the "accurate" values, it was enough to degrade the performance significantly. Although the NL controller with "inaccurate" parameters still performed on par with the basic PD controller, it is clear that it would not take a significantly larger error in the parameter values to cause the trajectory tracking performance to drop below the level attained by the basic PD controller.

TABLE VIII
PEAK MAGNITUDES AND FREQUENCIES OF ADDITIONAL SINUSOIDAL TRAJECTORIES

DOF	Magnitude	Frequency	Period	k_p	k_d
x_1	0.25 m	0.3925 rad/s	16 Seconds	500	200

TABLE IX
ADAPTATION GAINS FOR ϵANL CONTROLLER

DOF	γ_1	γ_2	γ_3	γ_4
x_1	5000	100000	0	10

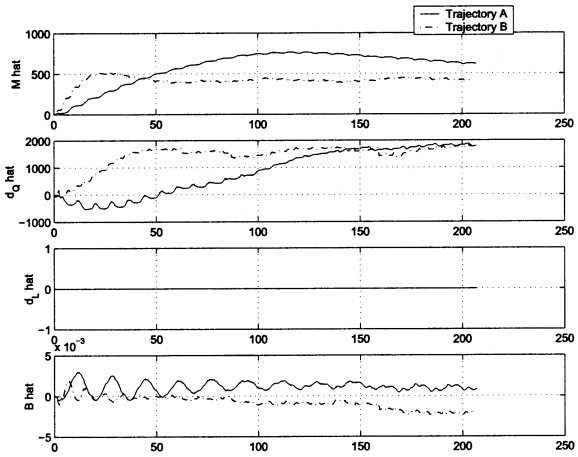

Fig. 19. Plot of adaptive parameter estimates using ANL controller to track trajectories in the x_1 DOF. Trajectory A is of peak magnitude 0.5m and frequency 0.3925 rad/s. Trajectory B is of peak magnitude 0.25m and frequency 0.785 rad/s. The graphs, top to bottom, are of the adaptive plant parameter estimates for effective mass ($\hat{m}(t)$), quadratic drag ($\hat{d}_Q(t)$), linear drag ($\hat{d}_L(t)$), and buoyancy ($\hat{b}(t)$).

We conclude that the performance of a model-based controller depends entirely on the accuracy of the dynamical plant model used in designing the controller. The results presented in this section clearly indicate that the tracking performance of the fixed model-based controllers is dependent on the accuracy of their models. If the plant model is incorrect, a model-based controller cannot be expected to perform better than a nonmodel-based controller, i.e., a PD controller. This section also directly corroborates the accuracy of the experimentally determined dynamical plant models for the JHUROV presented in Section II.

D. Effect of Different PD Gains

In this section, we examine the effect that different PD gains have on the tracking performance of the fixed model-based controllers. The JHUROV was commanded to track a trajectory the x_1, x_2, x_3, and x_4 DOFs, using the PD, EL, and NL controllers. The PD gains were adjusted such that we maintained a constant ratio $\zeta = k_d/(2\sqrt{mk_p})$. If the closed-loop system were a linear system, ζ would be the damping ratio. The four sets of PD gains used are listed in Table XI and the results are plotted in bar-chart format in Fig. 20.

As would be expected, trajectory tracking performance improved as the PD gains were increased. Conspicuously missing from Fig. 20 is data for the EL controller using gain sets D and

TABLE X
EFFECT OF MODEL PARAMETER ACCURACY

DOF	Controller	Inertia	D_Q	D_L	Buoyancy	X_{err} [rad]	V_{err} [rad/s]
x_4	PD (Good)	98.04	187.1	0	0.1197	0.0878	0.0714
x_4	EL (Good)	98.04	187.1	0	0.1197	0.0122	0.0255
x_4	NL (Good)	98.04	187.1	0	0.1197	0.00923	0.0151
x_4	NL (Bad)	200.0	100.0	0	0	0.0824	0.0664

TABLE XI
PD GAIN SET TABLE

Gain Set	DOF	k_p	k_d
A	1	250	141.4
B	1	500	200
C	1	1000	282.8
D	1	2000	400

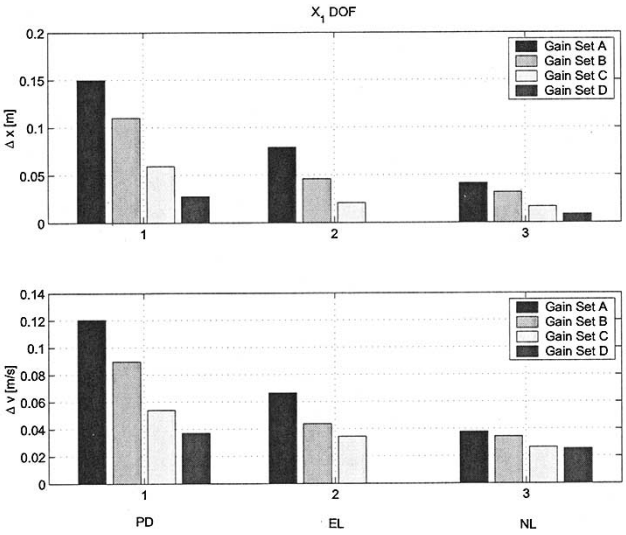

Fig. 20. Bar-chart plots of position tracking error (top) and velocity tracking error (bottom) for the PD (left), EL (center), and NL (right) controllers in the x_1 DOF. Gain sets are listed in Table XI. The reference trajectory is $x_d(t) = 0.25\cos(2 * \pi * (1/8) * t)$ [m]. $X_{\text{err}_1} = \text{mean}(|x_{d_1} - x_{p_1}|)$ [m], $V_{\text{err}_1} = \text{mean}(|v_{d_1} - v_{p_1}|)$ [m/s].

C, respectively. This is not an oversight; the JHUROV went unstable using this controller at these gains. This demonstrates the practical limit of increasing feedback gains. In theory, the gains may be adjusted infinitely high, but in practice such factors as discrete implementation, sensor limitations, and actuator response limit the value of the feedback gains. Fig. 20 further supports the performance trends reported in Sections V-A and B. The NL controller did the best job tracking the reference position and velocity trajectories, followed by the EL and the PD controllers. These observations are further supported by experiments run in the x_2, x_3, and x_4 DOF.

We conclude that the PD gains have a direct effect on the tracking performance of the fixed model-based controllers (EL and NL). As shown in this section, increasing the PD gains allowed for improvements in trajectory tracking. In addition, we again conclude that the fixed model-based controllers perform better than the basic PD controller. This section reinforces the operational limitation that while in theory the PD gains may be infinitely increased, in practice this has undesired effects such as instability.

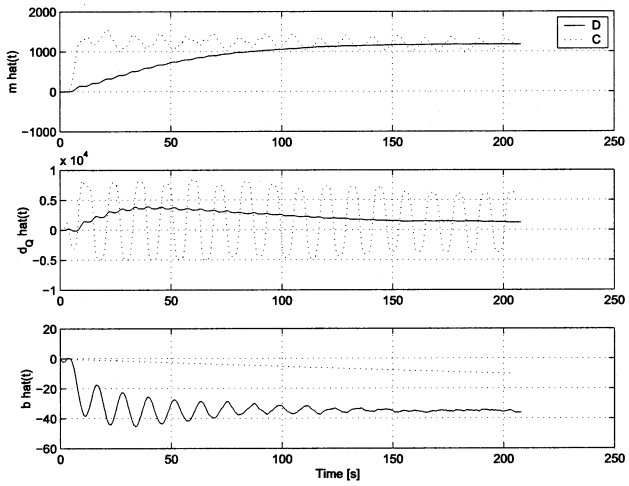

Fig. 21. Effect of adaptation gains on adaptive parameter estimates. Plot shows $\hat{m}(t)$, $\hat{d}_Q(t)$, and $\hat{b}(t)$ for two sets of adaptation gains using the ϵANL controller.

E. Effect of Adaptation Gains

How do different adaptation gains effect the performance of the adaptive model-based controllers? First, we examine the influence of the adaptation gains upon the adaptive parameter values and, second, the effect of the adaptation gains on tracking performance.

Dynamic vehicle trials were conducted in which the JHUROV used the ANL and ϵANL controllers, under several sets of adaptation gains, to track an identical sinusoidal reference trajectory of peak magnitude (0.2 m) and frequency (0.524 rad/s) in the x_3 DOF. During these experiments, the PD gains were kept constant at $k_p = 600$ and $k_d = 800$. The results of these experiments for two sets of adaptation gains are listed in Table XII. It is clear by looking at the plots of the adaptive parameter estimates in Fig. 21 that the adaptation gains directly effect the adaptive parameter estimates. For data set D, we see that all three adaptive parameter estimates converge to a value close to the value listed in Table III. However, we see that by increasing the γ_2 gain by a factor of 10 and decreasing the γ_4 gain by a factor of 50, as done in data set C, the estimated adaptive parameters behave much differently. The value for $\hat{b}(t)$ never reaches a final value. While the rise time for $\hat{m}(t)$ is much less in data set C, the tradeoff is that it oscillates significantly about a final value as opposed to the almost critically damped behavior seen in data set D. As for $\hat{d}_Q(t)$, we see that not only does it never reach a final value, it oscillates wildly. Similar differences in adaptive parameter value behavior were observed in the data sets using the ANL controller.

Despite the severe differences in the adaptive parameter behavior under the two different sets of adaptation gains, tracking

TABLE XII
EFFECT OF DIFFERENT ADAPTATION GAINS ON ADAPTIVE CONTROLLERS TRACKING PERFORMANCE. REFERENCE TRAJECTORY IS A SINUSOID OF PEAK MAGNITUDE 0.2 M AND FREQUENCY 0.524 rad/s. PD GAINS WERE $k_p = 600$ AND $k_d = 800$

Data Set	DOF	Controller	γ_1	γ_2	γ_3	γ_4	ϵ	$X_{err}[m]$	$V_{err}[m/s]$
A	x_3	ANL	50000	5000000	0	1	0	0.0627	0.0129
B	x_3	ANL	50000	500000	0	50	0	0.0529	0.0133
C	x_3	ϵANL	50000	5000000	0	1	1	0.0493	0.0234
D	x_3	ϵANL	50000	500000	0	50	1	0.0248	0.0195

performance is only marginally effected by the different adaptation gains. Looking at Table XII, we see that for both the ANL and ϵANL controllers, the tracking performance achieved by the adaptation gains in data sets B and D did slightly better than or on par with the tracking performance achieved using the adaptation gains in data sets A and C.

We conclude that the adaptation gains significantly effect the adaptive parameter estimates and their convergence. A wide range of adaptation gain values result in good trajectory tracking performance. This is consistant with the mathematical analysis reported in Section III. These conclusions are further supported by the data collected in the x_1, x_2, and x_4 DOFs.

F. Effect of Thruster Saturation

The theoretical stability analysis of the model-based controllers presented in Section III is based on the assumption that the actuators can deliver whatever force or torque the control law dictates. In the case of the JHUROV, this means that the thrusters need to be able to provide the required thrust or moment in the respective DOF. What happens when a thruster saturates and thus cannot meet the required level of thrust prescribed by the control law? Analytically, the stability proofs and theoretical predictions of the dynamic behavior offered in Section III no longer apply. To demonstrate the effects of thruster saturation, a trajectory was chosen for the JHUROV in the x_3 DOF that would saturate the thrusters in that DOF. This trajectory was run using the PD, EL, NL, AEL, and ANL controllers; the ϵANL was not run for this comparison. The PD feedback and adaptation gains were identical for each controller during these trials.

Comparing the results plotted in Fig. 22 with the results plotted for DOF x_3 in Fig. 16, it is clear that saturating the thrusters causes severe degradation in the tracking performance of the controllers. The fixed model-based controllers appear to handle this unmodeled effect the best, while the adaptive model-based controllers perform the worst with the thrusters saturating. Thruster saturation represents an unmodeled discontinuous dynamic. We surmise that this has a greater negative effect on the adaptive model-based controllers because, while they are not only based on an inaccurate model structure, as are the fixed model-based controllers, the adaptive model-based controllers also attempt to estimate the parameter values of that ill-structured plant model.

We conclude that thruster saturation greatly effects the performance of the model-based controllers. While the fixed model-base controllers (EL and NL) handled this unmodeled effect better than the adaptive model-based controller (AEL and ANL), all the controllers performed significantly worse with the thrusters saturating.

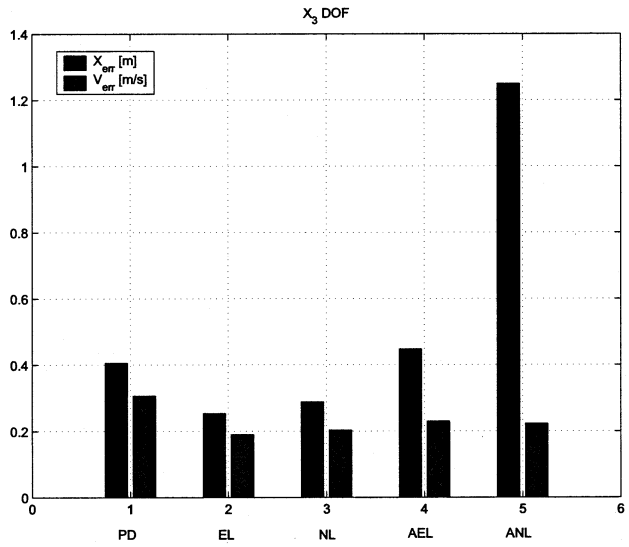

Fig. 22. Bar chart of position and velocity tracking error for the PD, EL, NL, AEL, and ANL controllers in the x_3 DOF. Reference trajectory was a sinusoid of peak magnitude 0.5 m and frequency 0.785 rad/s. The PD gains were $k_p = 600$ and $k_d = 800$ for each controller. The adaptation gains were $\gamma_1 = 50\,000$, $\gamma_2 = 5\,000\,000$, $\gamma_3 = 0$, and $\gamma_4 = 1$. $X_{\mathrm{err}_3} = \mathrm{mean}(|x_{d_3} - x_{p_3}|)$ [m], $V_{\mathrm{err}_3} = \mathrm{mean}(|v_{d_3} - v_{p_3}|)$ [m/s].

VI. CONCLUSION

This paper has reported a preliminary experimental evaluation of a family of model-based trajectory tracking controllers for the low-speed maneuvering of fully actuated underwater vehicles. We have considered the simple but empirically validated case of a decoupled plant dynamical model employing thrust input, constant added mass, constant linear and quadratic drag, and constant buoyancy. We have compared the performance of PD control, two fixed model-based controllers: an EL controller, an NL controller that does not exactly linearize, and the performance of the adaptive extensions of the fixed model-based controllers. These experiments of the closed-loop performance of these systems corroborate the theoretical and numerical predictions. Moreover, the experiments suggest that the model based controllers are robust with respect to: 1) sensor noise and inaccuracy; 2) thruster control accuracy; and 3) unmodeled plant dynamics. Specifically, the data indicates the following.

1) Fixed model-based controllers outperformed the PD controller in trajectory tracking.
2) NL controllers outperform EL controllers in trajectory tracking. We surmise that this performance difference is due to the fact that the EL controller attempts to exactly cancel NL plant drag terms relying on the plant model parameters to be *exactly* correct, whereas the NL controller

exploits the stabilizing property of the vehicle's natural quadratic damping.

3) Adaptive model-based controllers all provide accurate velocity tracking and the parameter estimates remain bounded and converge to fixed values. The addition of a position error feedback term to the adaptation update law in the ϵANL adaptive controller provides for accurate position tracking.
4) Increasing PD feedback gains improves the tracking performance of all controllers uniformly, but in general preserves their relative performance ranking—i.e., the model-based controllers outperform PD control. The EL controller is sensitive to unmodeled dynamics and sensor noise at high feedback gains.
5) Model-based controllers perform well over a wide range of reference trajectories within the plant's actuator saturation limits. Adaptive model parameter convergence is faster for trajectories with high velocities and accelerations.
6) When fixed model-based controllers employ incorrect plant model parameters, their performance suffers severely.
7) Adaptation gains significantly effect the adaptive parameter estimates and their convergence. At present, tuning adaptation gains remains a "black art" for which we have little analytical insight.
8) Thruster saturation significantly degrades the performance of the model-based controllers. While the fixed model-based controllers (EL and NL) handled this unmodeled effect the better than the adaptive model-based controller (AEL and ANL), the performance of all controllers degrades significantly in the presence of thruster saturation.

ACKNOWLEDGMENT

The authors gratefully acknowledge their collaboration with Dr. D. Stilwell, formerly with the U.S. Naval Academy, Annapolis, MD, and currently with the Virginia Polytechnic Institute and State University, Blacksburg. Dr. Stilwell deployed his IMU on the vehicle during these experiments to examine the issue of IMU calibration. They are grateful to the faculty and staff of the U.S. Naval Academy Hydromechanics Laboratory for their world-class testing facilities; to Dr. D. Yoerger of the Woods Hole Oceanographic Institution, Woods Hole, MA, who graciously provided use of his 300-kHz SHARPS acoustic transponder system; and to Dr. H. Singh of the Woods Hole Oceanographic Institution, who graciously provided use of his Paroscientific depth sensor upon the untimely demise of our depth sensor during these experimental trials.

REFERENCES

[1] A. Alessandri, M. Caccia, G. Indiveri, and G. Veruggio, "Application of LS and EKF techniques to the identification of underwater vehicles," in *Proc. IEEE Int. C. Control Applications*, Trieste, Italy, 1998, pp. 1084–1088.

[2] C. H. An, C. G. Atkeson, and J. M. Hollerbach, "Experimental determination of the effect of feedforward control on trajectory tracking errors," in *Proc. IEEE Int. Conf. Robotics and Automation*, San Francisco, CA, 1986, pp. 55–60.

[3] G. Antonelli, F. Caccavale, S. Chiaverini, and L. Villani, "Tracking control for underwater vehicle-manipulator systems with velocity estimation," *IEEE J. Oceanic Eng.*, vol. 25, pp. 399–413, July 2000.

[4] G. Antonelli, S. Chiaverini, N. Sarkar, and M. West, "Adaptive control of an autonomous underwater vehicle: Experimental results on ODIN," in *Proc. 1999 IEEE Int. Symp. Computational Intelligence in Robotics and Automation*, Monterey, CA, 1999, pp. 64–69.

[5] ——, "Adaptive control of an autonomous underwater vehicle: Experimental results on ODIN," *IEEE Trans. Contr. Syst. Technol.*, vol. 9, pp. 756–65, Sept. 2001.

[6] S. Arimoto and F. Miyazaki, "Stability and robustness of PID feedback control for robot manipulators of sensory capability," in *Proc. Robotics Research, First Int. Symp.*, Cambridge, MA, 1984.

[7] R. Bachmayer, L. L. Whitcomb, and M. Grosenbaugh, "An accurate four-quadrant nonlinear dynamical model for marine thrusters: Theory and," *IEEE J. Oceanic Eng.*, vol. 25, pp. 146–159, Jan. 2000.

[8] M. Caccia, G. Bruzzone, and G. Veruggio, "Guidance of unmanned underwater vehicles: Experimental results," in *Proc. IEEE Int. Conf. Robotics and Automation*, San Francisco, CA, 2000, pp. 1799–1804.

[9] M. Caccia, G. Indiveri, and G. Veruggio, "Modeling and identification of open-frame variable configuration underwater vehicles," *IEEE J. Oceanic Eng.*, vol. 25, pp. 227–240, Apr. 2000.

[10] S. K. Choi and J. Yuh, "Experimental study on a learning control system with bound estimation for underwater robots," in *Proc. IEEE Int. Conf. Robotics and Automation*, Apr. 1996, pp. 2160–2165.

[11] J. L. Christensen, "LBL NAV—[Long Base Line Navigation]—An acoustic transponder navigation system," in *Proc. IEEE OCEANS'79*, San Diego, CA, Sept. 1979, pp. 507–512.

[12] J. J. Craig, *Adaptive Control of Mechanical Manipulators*. Reading, MA: Addison-Wesley, 1988.

[13] J. J. Craig, P. Hsu, and S. Sastry, "Adaptive control of mechanical manipulators," *Int. J. Robot. Res.*, vol. 6, no. 2, pp. 16–28, 1987.

[14] R. Cristi, F. A. Papoulis, and A. J. Healey, "Adaptive sliding mode control of autonomous underwater vehicles in the dive plane," *IEEE J. Oceanic Eng.*, vol. 15, pp. 152–160, July 1990.

[15] J. P. V. S. da Cunha, R. R. Costa, and L. Hsu, "Design of a high performance variable structure position control of ROV's," *IEEE J. Oceanic Eng.*, vol. 20, pp. 42–55, Jan. 1995.

[16] K. S. M. Davidson and L. I. Schiff, "Turning and course keeping qualities," *Trans. Soc. Naval Architects Marine Eng.*, vol. 54, pp. 152–200, 1946.

[17] *LORAN-C Users Handbook*, 1992 ed., U.S. Coast Guard, Washington, DC, 1992.

[18] S. Dubowsky and D. T. DesForges, "The application of modelreference adaptive control to robotic manipulators," *ASME J. Dynamic Syst., Measur., Contr.*, vol. 101, no. 3, pp. 193–200, 1979.

[19] S. Eiani-Cherif, G. Lebret, and M. Perrier, "Identification and control of a submarine vehicle," in *Proc. 5th IFAC Symp. Robot Contr.*, Nantes, France, 1997, pp. 307–312.

[20] J. A. Farrell and M. Barth, *The Global Positioning System and Inertial Navigation*. New York: McGraw-Hill, 1999.

[21] J. P. Feldman, "State-of-the-art for predicting the hydrodynamic characteristics of submarines," in *Proc. Symp. Contr. Theory Naval Applicat.*, Monterey, CA, June 1975, Defense Tech. Inform. Center doc. A071 804, pp. 87–127.

[22] ——, "DTNSRDC Revised Standard Submarine Equations of Motion," David Taylor Naval Ship Research and Development Center, Defense Tech. Inform. Center doc. A071 804, 1979.

[23] T. I. Fossen, *Guidance and Control of Ocean Vehicles*. New York: Wiley, 1994.

[24] T. I. Fossen and S. I. Sagatun, "Adaptive control of nonlinear underwater robotic systems," in *Proc. IEEE Int. Conf. Robotics Automation*, Sacramento, CA, 1991, pp. 1687–94.

[25] E. Freund, "Fast nonlinear control with arbitrary pole placement for industrial robots and," *Int. J. Robot. Res.*, vol. 1, no. 1, pp. 65–78, 1982.

[26] M. Gertler and G. Hagen, "Standard Equations of Motion for Submarine Simulation," David Taylor Naval Ship Research and Development Center, Defense Tech. Inform. Center doc. 653 861, 1967.

[27] K. Goheen and E. Jefferys, "The application of alternative modeling techniques to ROV dynamics," in *Proc. IEEE Int. Conf. Robotics Automation*, May 1990, pp. 1302–1309.

[28] K. G. Goheen and E. R. Jefferys, "On the adaptive control of remotely operated underwater vehicles," *Int. J. Adaptive Contr. Signal Process.*, vol. 4, no. 4, pp. 287–97, July/Aug. 1990.

[29] K. R. Goheen and E. R. Jeffereys, "Multivariable self-tuning autopilots for autonomous and remotly operate underwater vehicles," *IEEE J. Oceanic Eng.*, vol. 15, pp. 144–151, July 1990.

[30] A. Goodman, "Experimental techniques and methods of analysis used in submerged body research," in *Proc. Third Symp. Naval Hydrodynamics*, Washington, DC, 1960, pp. 379–449.
[31] A. J. Healey, "Model-based maneuvering controls for autonomous underwater vehicles," *ASME J. Dynamic Syst., Measur., Contr.*, vol. 114, no. 4, pp. 614–622, 1992.
[32] A. J. Healey, P. E. An, and D. B. Marco, "Online compensation of heading sensor bias for low cost AUV's," in *Proc. 1998 Workshop Autonomous Underwater Vehicles*, Cambridge, MA, Aug. 1998, pp. 35–42.
[33] A. J. Healey and D. Lienard, "Multivariable sliding mode control for autonomous diving and," *IEEE J. Oceanic Eng.*, vol. 18, pp. 327–339, July 1993.
[34] A. J. Healey, S. M. Rock, S. Cody, D. Miles, and J. P. Brown, "Toward an improved understanding of thruster dyamics for underwater vehicles," *IEEE J. Oceanic Eng.*, vol. 20, pp. 354–61, Oct. 1995.
[35] R. Horowitz and M. Tomizuka, "An adaptive control scheme for mechanical manipulators—Compensation of nonlinearity and decoupling control," *ASME J. Dynamic Syst., Measur., Contr.*, vol. 108, pp. 127–135, 1986.
[36] L. Hsu, R. R. Costa, F. Lizarralde, and J. P. V. S. da Cunha, "Dynamic positioning of remotely operated underwater vehicles," *IEEE Robot. Automat. Mag.*, vol. 7, pp. 21–31, Sept. 2000.
[37] M. M. Hunt, W. M. Marquet, D. A. Moller, K. R. Peal, W. K. Smith, and R. C. Spindell, "An acoustic navigation system," Woods Hole Oceanogr. Inst., Woods Hole, MA, Tech. Rep. WHOI-74-6, 1974.
[38] T. W. Kim and J. Yuh, "A novel nuero-fuzzy controller for autonmous underwater vehicles," in *Proc. IEEE Int. Conf. Robotics and Automation*, May 21–26, 2001, pp. 2350–55.
[39] D. E. Koditschek, "High gain feedback and telerobotic tracking," in *Proc. Workshop on Space Telerobotics*, Pasadena, CA, Jan. 1987, pp. 355–363.
[40] H. N. Koivo, "A multivariable self-tuning controller," *Automatica*, vol. 16, no. 4, pp. 351–66, 1980.
[41] L. Larsson, B. Regnstrom, L. Broberg, D. Li, and C. Janson, "Failures, fantasies, and feats in the theoretical/numerical prediction of ship performance," in *Proc. 22nd Symp. Naval Hydrodynamics*, Washington, DC, 2000, pp. 11–32.
[42] J. P. Lasalle and S. Lefschetz, *Stability by Lyapunov's Direct Method with Applications*. New York: Academic, 1961.
[43] A. Lawrence, *Modern Inertial Technology*. New York: Springer-Verlag, 1993.
[44] N. Leonard, "Stability of a bottom-heavy underwater vehicle," *Automatica*, vol. 33, no. 3, pp. 331–46, 1997.
[45] J. Y. S. Luh, M. W. Walker, and R. P. C. Paul, "On-line computational scheme for mechanical manipulators," *ASME J. Dyn. Syst., Measur., Contr.*, vol. 102, no. 2, pp. 69–76, 1980.
[46] ——, "Resolved-acceleration control of mechanical manipulators," *IEEE Trans. Automat.Contr.*, vol. AC-25, pp. 468–474, June 1980.
[47] P. H. Milne, *Underwater Acoustic Positioning Systems*. Houston, TX: Gulf, 1983.
[48] D. A. Mindell, "Datum for its own annihilation: Feedback, control, and computing 1916–1945," Ph.D. dissertation, Massachusetts Inst. Technol., Cambridge, 1996.
[49] A. T. Morrison III and D. R. Yoerger, "Determination of the hydrodynamic parameters of an underwater vehicle during small scale, nonuniform, 1-dimensional translation," *Proc. IEEE/MTS OCEANS'93*, pp. 277–282, Oct. 1993.
[50] K. Narendra and A. Annaswamy, *Stable Adaptive Systems*. New York: Prentice-Hall, 1988.
[51] N. Sadegh and R. Horowitz, "Stability and robustness analysis of a class of adaptive controllers for robotic manipulators," *Int. J. Robot. Res.*, vol. 9, no. 3, pp. 74–92, 1990.
[52] J.-J. E. Slotine and W. Li, "On the adaptive control of robot manipulators," in *Proc. ASME Annual Winter Meet.*, Anaheim, CA, 1986, pp. 51–56.
[53] ——, "On the adaptive control of robot manipulators," *Int. J. Robot. Res.*, vol. 6, no. 3, pp. 49–59, 1987.
[54] D. Smallwood, R. Bachmayer, and L. Whitcomb, "A new remotely operated underwater vehicle for dynamics and control research," in *Proc. 11th Int. Symp. Unmanned Untethered Submersible Technology*, Durham, NH, 1999, pp. 370–377.
[55] D. A. Smallwood, "Advances in Dynamical Modeling and Control of Underwater Robotic Vehicles," Ph.D. dissertation, The Johns Hopkins Univ., Baltimore, MD, 2003.
[56] D. A. Smallwood and L. L. Whitcomb, "Preliminary experiments in the adaptive identification of dynamically positioned underwater robotic vehicles," in *Proc. 2001 IEEE/RSJ Int. Conf. Intelligent Robots and Systems*, Maui, HI, 2001, pp. 1803–1810.
[57] ——, "Adaptive identification of dynamically positioned underwater robotic vehicles," *IEEE Trans. Contr. Syst. Technol.*, vol. 11, pp. 505–515, July 2003.
[58] M. Takegaki and S. Arimoto, "An adaptive trajectory control of manipulators," *Int. J. Contr.*, vol. 34, no. 2, pp. 219–230, 1981.
[59] J. van Amerongen, P. van der Klugt, and H. van Nauta Lemke, "Rudder roll stabilization for ships," *Automatica*, vol. 26, no. 4, pp. 679–690, 1990.
[60] J.-S. Wang, C. Lee, and J. Yuh, "Self-adaptive neuro-fuzzy systems with fast parameter learning for autonomous underwater vehicle control," in *Proc. IEEE Int. Conf. Robotics and Automation*, May 2000, pp. 3861–3866.
[61] J. T. Wen and D. S. Bayard, "Robust control for robotic manipulators Part I: Non-adaptive case," Jet Propulsion Lab., Pasadena, CA, Tech. Rep. 347-87-203, 1987.
[62] L. L. Whitcomb, A. Rizzi, and D. E. Koditschek, "Comparative experiments with a new adaptive controller for robot arms," *IEEE Trans. Robot. Automat.*, vol. 9, pp. 59–70, Feb. 1993.
[63] D. R. Yoerger and J. E. Slotine, "Adaptive sliding control of an experimental underwater vehicle," in *Proc. IEEE Int.l Conf. Robotics and Automation*, Sacremento, CA, Apr. 1991, pp. 2746–2751.
[64] D. R. Yoerger and J.-J. E. Slotine, "Robust trajectory control of underwater vehicles," *IEEE J. Oceanic Eng.*, vol. OE-10, pp. 462–70, Oct. 1985.
[65] J. Yuh, J. Nie, and C. Lee, "Experimental study on adaptive control of underwater robots," in *Proc. IEEE Int. Conf. Robotics and Automation*, May 1999, pp. 393–398.

David A. Smallwood (S'01–M'04) received the B.S. degree from the University of Miami, Coral Gables, FL, in 1997 and the M.S. and Ph.D. degrees from The Johns Hopkins University, Baltimore, MD, in 1999 and 2003, respectively, all in mechanical engineering.

He conducted his Ph.D. research in the Dynamical Systems and Controls Laboratory, Department of Mechanical Engineering, The Johns Hopkins University. His Ph.D. research involved the dynamics and control of underwater robotic vehicles. As part of this work, he designed and built the JHUROV, a remotely operated vehicle used for research in underwater vehicle navigation, dynamics, and control. He is a Senior Electro-Mechanical Engineer in the Systems Engineering Department, Diagnostic Products Corporation, Instrument Systems Division, Flanders, NJ.

Louis L. Whitcomb (S'90–M'93–SM'02) received the B.S. and Ph.D. degrees from Yale University, New Haven, CT, in 1984 and 1992, respectively.

From 1984 to 1986, he was an R&D Engineer with the GMFanuc Robotics Corporation, Troy, MI. From 1992 to 1994, he was a Postdoctoral Fellow at the Woods Hole Oceanographic Institution, Woods Hole, MA, and at the University of Tokyo, Tokyo, Japan. He holds numerous patents in the field of robotics. His research focuses on the design, dynamics, and control of nonlinear dynamical systems. He is an Associate Professor in the Department of Mechanical Engineering, with a joint appointment in the Department of Computer Science, at The Johns Hopkins University, Baltimore, MD.